Chapter 2
Radiation in Space: The Physics

Abstract The radiation field in space is highly variable in time and space. Different sources contribute to the total exposure. In interplanetary space, the field is dominated by the omni-present galactic cosmic radiation (GCR) and sporadic solar particle events (SPE) can contribute. On the International Space Station (ISS) in low Earth orbit (LEO), on the other hand, the contribution of SPE can be neglected and GCR are modulated along the station's trajectory due to the shielding effect of the geomagnetic field against charged particles. On planetary surfaces, for instance, on Mars, albedo particles from underground and secondary particles from interactions with the atmosphere, if present, are added to the radiation field. Secondary particles, especially neutrons, can contribute significantly to the exposure. In all cases, the field can be further modified by the potential shielding environment and the resulting particle fluxes lead to the exposure of humans under the given conditions. The exposure is calculated as the energy deposition in tissue weighted with corresponding quality factors or relative biological effectiveness and organ weighting factors. In most cases, if measured, the dose rate is determined from the energy deposition in silicon detectors and corresponding corrections have to be applied to estimate the dose in tissue. Additionally, self-shielding of the body has to be taken into account if organ doses are determined.

Keywords Galactic cosmic rays (GCR) · Solar particle events (SPE) · Van Allen Belts · Absorbed dose · Dose equivalent · Effective dose equivalent · Anthropomorphic phantoms · Passive detectors · Active detectors · Radiation exposure

C. E. Hellweg et al., *Radiation in Space: Relevance and Risk for Human Missions*, SpringerBriefs in Space Life Sciences,
https://doi.org/10.1007/978-3-030-46744-9_2

2.1 The Radiation Field

Every human being is permanently exposed to natural radiation. For the majority of humankind, the largest part of this radiation stems from naturally occurring ambient radioactive nuclei in the soil or their decay products. The contribution of cosmic radiation to the total natural exposure is approximately 15% on average (UNSCEAR (2000) gives an average value for the yearly effective dose from cosmic radiation of 380 μSv and a total of 2.4 mSv). The actual value depends among others on the altitude, the local soil composition, and diet.

Under certain conditions, however, the contributions of radiation which originates not from Earth but from space increases and may become the only relevant factor. The sources of this radiation are threefold: atomic nuclei that are accelerated to extremely high energies at extra-heliospheric sources in the galaxy, the galactic cosmic radiation (GCR), protons and electrons that are accelerated in solar flares or coronal mass ejections close to the visible solar surface or in interplanetary space, the solar energetic particles (SEP); and protons and electrons temporarily trapped in the magnetic field of Earth in the radiation belts. The nature of this radiation differs from radiation sources found on Earth in energy and composition. Heavy ions in the GCR have a high biological effectiveness, and they reach energies at which it is impossible to shield against them under the current technical constraints in human spaceflight. The interaction of the primary radiation with shielding material creates a complex field of secondary radiation containing an increasingly large fraction of neutrons. Energies of particles from the radiation sources encountered in space usually have much greater energies than typical terrestrial sources. Alpha particles (fully ionized He nuclei) originating from radioactive decay, for instance, have kinetic energies on the order of MeV, the energies of those from GCR exceed tens and even hundreds of GeV which allows them to penetrate shielding that is orders of magnitude thicker compared to what is needed to shield alpha particles from radioactive decay.

Figure 2.1 gives an overview over the energy regimes of different sources of radiation in space. Sources that are potentially relevant for the exposure to ionizing radiation are trapped protons and electrons (during extravehicular activities) in low Earth orbit (LEO), protons of solar origin, and galactic cosmic radiation.

2.1.1 Galactic Cosmic Rays

Galactic cosmic rays (or synonymously used: galactic cosmic radiation (GCR)) consist of highly energetic particle radiation that enters the heliosphere from interstellar space and originates at galactic sources like supernova remnants (Blasi 2013). The intensity of GCR in the interstellar space is considered to be effectively constant over time and outside the heliosphere, the intensity of GCR is described by the local interstellar spectra. On their way to a given location in the heliosphere, the shape of the GCR spectra changes through the interaction of the charged particles

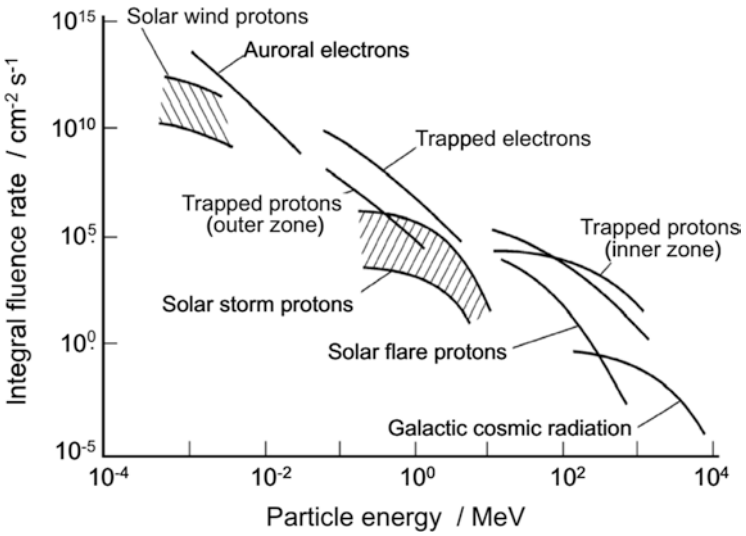

Fig. 2.1 Approximate energy ranges and spectra of different components of the radiation field in space. (From Wilson 1978)

with the magnetic field in the interplanetary medium. The strength of this effect depends primarily on the particle's energy and charge and on the activity of the Sun and the related solar wind velocity and is accordingly strongest during periods of strong solar activity (solar maximum) and weakest during low solar activity (solar minimum). This leads to a GCR intensity that is anti-correlated with solar activity showing intensity maxima at times of low solar activity and vice versa.

For the radiation exposure in space, only the hadronic part of the GCR is relevant. The intensity of electrons and positrons in the GCR is on the order of 1–2% (Boezio et al. 1999, 2000), and the dose is even lower as the dose per fluence is, depending on the particle energy, significantly lower than for protons and heavier ions. The hadronic part consists mainly of protons (≈87%), alpha particles (≈12%), and to a lesser extent of heavier ions (Simpson 1983). Even though the abundance of heavier ions is low, their contribution to the exposure is significant and accurate consideration in measurements and models is crucial. Model predicted GCR abundances in near-Earth interplanetary space and averaged over the ISS orbit are illustrated in Fig. 2.2.

The relevant energy range for the exposure from GCR depends on the specific shielding environment but typically ranges from approximately 100 MeV/n to 100 GeV/n (Mrigakshi et al. 2013a).

For heavily shielded environments including additional magnetic shielding energies up to 1 TeV/n can become relevant. This is the case, for instance, for low latitude flights in aviation.

In the energy spectrum above a few ten GeV up to 1 TeV, the GCR energy spectra follows a power law with a spectral index of approximately −2.7 (Blasi 2013) but a more detailed consideration shows that the index is neither constant for different

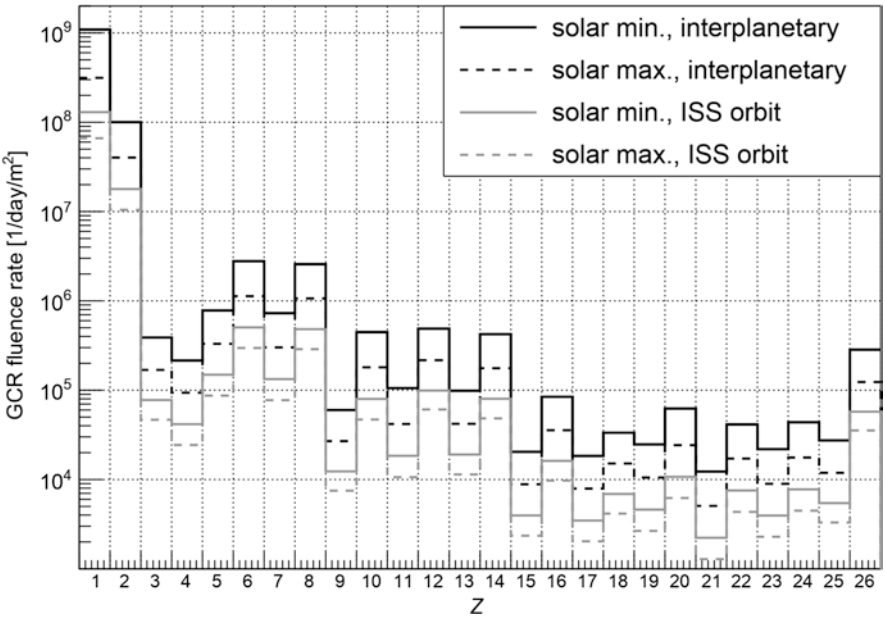

Fig. 2.2 Particle fluence rate for GCR with charge number $Z = 1$ (hydrogen) to 26 (iron) during solar maximum and minimum conditions in near-Earth interplanetary space and at the orbit of the International Space Station (ISS) as predicted by the model by Matthiä et al. (2013)

energies nor identical for all GCR particles (Adriani et al. 2011; Aguilar et al. 2015a, b), for instance, showing a hardening of the proton spectrum above 200 GeV (Aguilar et al. 2015b). At even higher energies above the so-called knee at around $3 \bullet 10^6$ GeV, the energy spectrum becomes steeper. At energies below a few ten GeV, the spectrum gradually bends over showing a maximum at around 500 MeV/n. This region is strongly affected by the solar modulation and varies in intensity during the solar cycle. Figure 2.3 illustrates the GCR spectra of hydrogen (proton), helium (alpha), and iron nuclei as described by the models of Matthiä et al. (2013) and Badhwar-O-Neill 2014 (NASA 2015) for solar minimum and maximum conditions during the years 2010 and 1991, respectively. Data for the Badhwar-O'Neill model have been taken from NASA's OLTARIS tool (*oltaris.nasa.gov*). The variation in the GCR flux at 100 MeV/n is about one order of magnitude and decreasing with increasing energy. Particles with energies above a few tens of GeV/n are almost unaffected by solar modulation. The total fluence rate integrated over energies between 10 MeV/n and 200 GeV/n of nuclei from H ($Z = 1$) and Fe ($Z = 26$) for solar minimum and maximum and for interplanetary space and ISS orbit is given in Fig. 2.3. It shows that hydrogen nuclei are more affected by solar modulation than heavier nuclei and that the variation in the ISS orbit is much weaker than in interplanetary space. The latter is a consequence of the magnetic shielding in the ISS orbit deflecting a significant part of the lower energetic primary particles which are most affected by the solar modulation. The total fluence in the average ISS orbit is

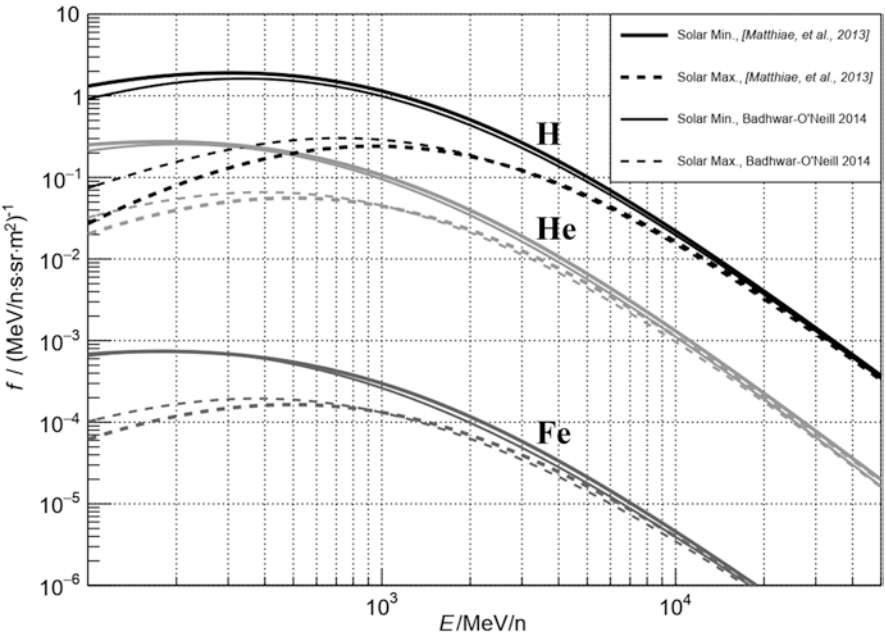

Fig. 2.3 GCR spectra of protons (H), alpha particles (He), and Fe ions for solar minimum and maximum as described by two models: Matthiä et al. (2013) and Badhwar-O-Neill 2014 (NASA 2015)

reduced by about one order of magnitude compared to interplanetary space which is a combined result of the magnetic shielding and the shielding provided by the Earth.

The variation in the GCR intensity over the solar cycle translates to changes in the radiation exposure in space, the magnitude of which depend on the shielding situation and the dose quantity. Mrigakshi et al. (2013b) have estimated that in a lightly shielded environment the variation between the most extreme GCR minimum and maximum in the past decades was expected to be about a factor of 3 for interplanetary space and about a factor of 2 for an average ISS orbit. NASA (1999) gave similar values for an unshielded interplanetary environment and predicted decreasing amplitude for increasing mass shielding. The mass shielding in interplanetary space has a similar effect as the magnetic shielding in a low inclination LEO: it reduces the relative contribution of lower energetic primary GCR which are the cause for the solar modulation-driven variation in the dose rates. It is evident that the estimation of the exposure from GCR depends on the accuracy of the underlying GCR model. Mrigakshi et al. (2013a) and Slaba and Blattnig (2014) have investigated the effect of applying different primary GCR models in the prediction of the radiation exposure. The results showed that differences in the predicted dose rates using different models for the primary GCR can easily exceed 50% if the GCR model is not sufficiently benchmarked.

2.1.2 Solar Radiation

While the Sun produces electromagnetic radiation over a wide range of wavelengths permanently, the production of solar energetic particles (SEPs) is limited to sporadic events which can last between hours and days. The origins of the energetic particles are active regions on or close to the visible surface of the Sun, solar flares, or coronal mass ejections (CMEs) close to the Sun or in interplanetary space. During these events, charged particles, mostly electrons and protons and a minor fraction of heavier ions, are accelerated to relativistic energies. Impulsive events in which particles are accelerated in magnetic reconnection events in the solar flare last several hours and are of minor relevance for radiation exposure due to their shorter duration and lower fluence compared to gradual events in which the particles are accelerated in the shock accompanying the CME. These events are longer lasting and typically contain a larger fraction of highly energetic protons (Reames 2013; Desai and Giacalone 2016). For radiation exposure purposes typically, only protons are considered and other particles are neglected. The characteristics of SEP events as they are observed at Earth vary significantly from event to event and depend on a number of factors such as the magnetic connection of the observer to the shock front, the CME speed and the conditions of the ambient interplanetary medium. Larger particle fluence typically correlates with faster CMEs speeds and events which are observed on the western hemisphere of the Sun. The time profile of the particle flux during an event depends on the energy that is considered and how the observer is connected to the source of the energetic particles (Reames 1999; Cane and Lario 2006). The rise time between the onset of the event and the peak of the particle flux can be between minutes and days and also the durations of events vary. For relatively low energies up to tens of MeV, the maximum may be reached only when the shock driven by the CME passes the observer. These are called energetic storm particles (ESP).

The energy spectrum of the SEPs reaches from the keV region up to several hundred MeV. Protons during the most intense of these events can even reach kinetic energies of several GeV and if the particle fluence is great enough, the increased intensity of cosmic radiation can also be recorded on ground by neutron monitor stations (Simpson 2000). These events are then called ground level events or enhancements (GLE). In recent decades, GLEs have occurred on average approximately once a year with an increased frequency of occurrence during periods of high solar activity. Between 2010 and 2020, however, only two such events have been recorded, on 17 May 2012 and 10 September 2017 which is a consequence of the modest solar activity in the current solar cycle. Solar particle events with lower intensity and particle energy are more frequent and Gopalswamy et al. (2015) list 37 large SEP events between Aug 2010 and Nov 2014 which is still a low number compared to previous solar cycles. The energy spectrum of the protons can be described by a single or double power law in energy or rigidity. The slope of the spectrum is of great importance for the impact of the event on radiation exposure. Soft spectra with a large fraction of lower energetic particles are more easily

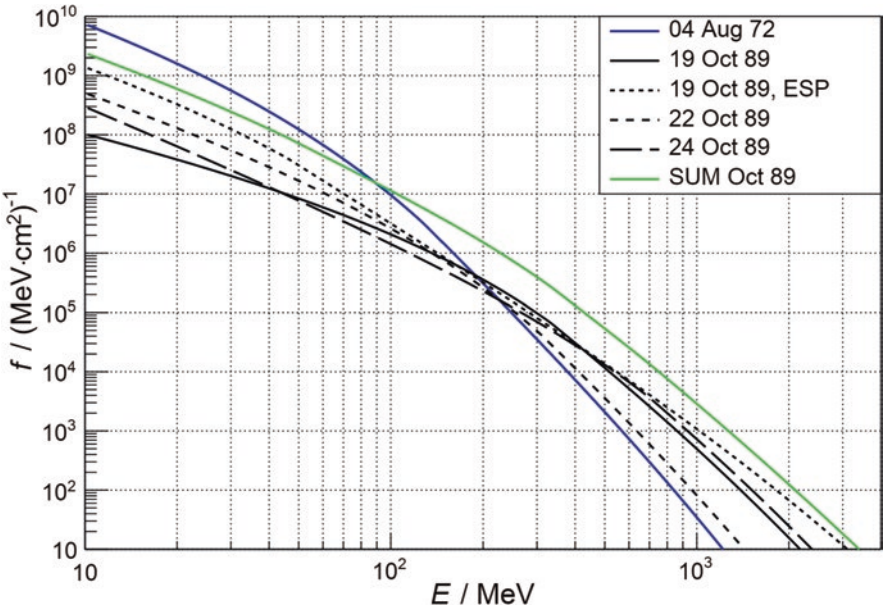

Fig. 2.4 Energy spectra of selected large SEP events as described by Tylka et al. (2010)

shielded by mass or by a magnetic field and the radiation exposure in the human body is expected to be less homogeneous than in case of a hard event which contains a relatively larger fraction of highly energetic particles.

Figure 2.4 illustrates the event integrated differential fluence spectra derived from Tylka et al. (2010) who described the integral proton spectrum by a double power law in rigidity with an exponential turnover (Band et al. 1993). The sum of the October 1989 events was recommended to NASA by Townsend et al. (2018) to be used as standard in designing storm shelters against solar particle events space habitats.

The October 1989 event had a comparatively hard spectrum meaning that it contained a large fraction of highly energetic protons with energies above a few hundred MeV. These particles can penetrate moderate or even heavy shielding (the range of 200 MeV protons in Al is approximately 120 mm and of 1 GeV protons approximately 1.5 m) and contribute to the exposure directly but with reduced intensity. Townsend et al. (2018) estimated that organ dose rate for the combined Oct 1989 event would exceed the exposure limit of 250 milliGray-Equivalent (mGy-Eq, see 2.2.1) for shielding below approximately 10 g/cm^2 Al (≈4 cm). Softer events may have greater fluence at lower energies which could lead to higher doses for lightly shielded conditions, for instance, during an EVA. The total dose that is to be expected is always a combination of the particle spectra, the temporal profile, and the exposure time under the specific shielding conditions. For instance, the dose from a soft event could be greater for a lightly shielded environment than the dose from a hard event if the fluence at low energies is higher. For the identical events

encountered at heavier shielded locations, on the other hand, the situation may be inverted and the greater number of highly energetic particles in the spectrum of the hard event may lead to the higher doses. The total dose to which an astronaut would be exposed to during an event is a complex combination of the event characteristics, for instance, onset to peak rise time, spectral hardness, and total duration, and the specific exposure conditions like shielding environment and duration of stay at different locations. During large events with a short rise time and a sharply peaked maximum, for instance, it is more important for the astronaut to reach a better shielded location (a radiation shelter) quickly than for an event which may have a similar total fluence but a longer rise time with a less sharply peaked maximum.

General statements on the impact of SEP events on the dose are therefore hard to make but most numerical estimates of the expected dose rates agree that for interplanetary space a mass shielding equivalent to approximately 10–20 g/cm^2 is sufficient to reduce the exposure below current thresholds (Townsend et al. 2018). For other exposure scenarios, like LEO, Moon, or Mars surface, the required mass is reduced due to the additional shielding provided by the magnetosphere, the atmosphere, and the planet.

As the occurrence frequency of SEP events varies over the solar cycle and also from cycle to cycle, probabilistic models can be used to estimate the risk for astronauts to be exposed to an event of a specific magnitude for a certain mission scenario depending on the size of the event, the length of the mission, and the launch date relative to the solar cycle, e.g., Xapsos et al. (2000), Kim et al. (2009), Jiggens et al. (2018).

2.1.3 Radiation Belt Particles

The term radiation belt refers to regions surrounding Earth, or more generally any planet with a global magnetic field, and containing highly energetic charged particles, mainly protons and electrons. These energetic particles are temporarily trapped in the magnetosphere in toroidal structures that stretch, in case of Earth, from a few hundreds of kilometers above ground out to several ten thousands of kilometers. The radiation belts are dynamical structures which are affected by space weather, for instance, by the solar wind pressure, heliospheric magnetic field, and GCR intensity (Baker et al. 2018). Typically, Earth is surrounded by two radiation belts, an inner and an outer belt (Fig. 2.5). The inner belt contains mostly protons with energies up to several GeV and a small fraction of electrons. The dominant source of high energy protons in the inner radiation belt is the cosmic ray albedo neutron decay (CRAND) process (Jentsch 1981) but other sources can contribute.

Depending on altitude and inclination, objects in an Earth orbit may cross the radiation belts several times per day and may be exposed to varying intensities of radiation belt particles with a wide range of energies. Of special interest for human

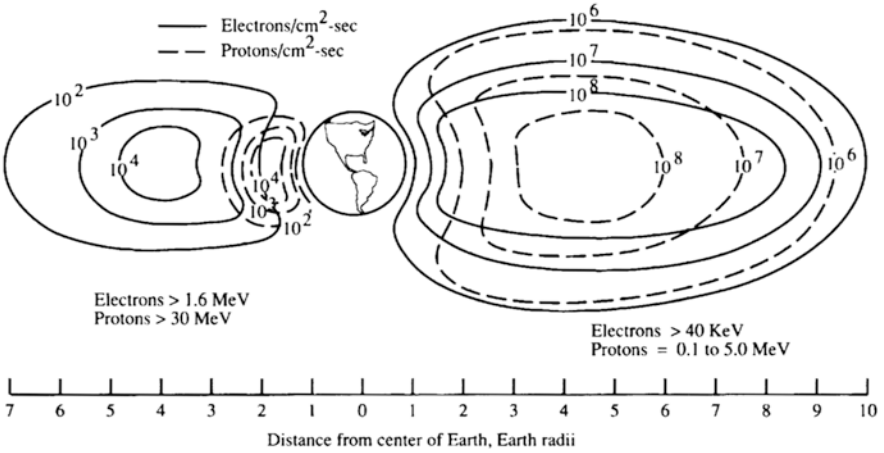

Fig. 2.5 Particle fluence rates of electrons and protons in the inner and outer radiation belts. (From NASA 1991)

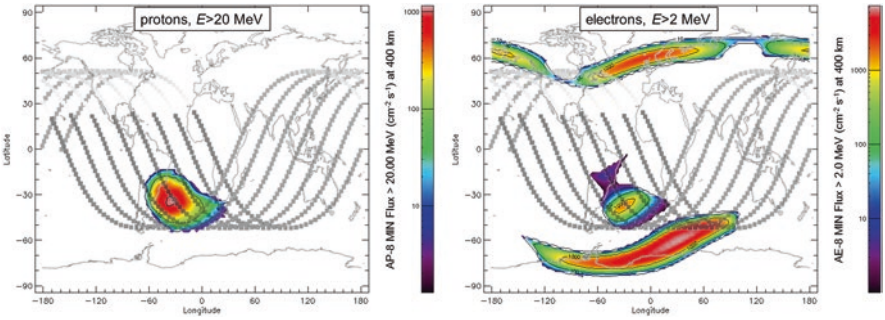

Fig. 2.6 Trapped protons (left) and electrons (right) in the radiation belts as predicted by the AP8 model in SPENVIS (www.spenvis.oma.be) at an altitude of 400 km, the approximate altitude of the ISS. The overlays show several passes of an orbit of 51.6° inclination

spaceflight is an area above the south-eastern part of South America and the South Atlantic, the so-called South Atlantic Anomaly (SAA). In this area, the inner radiation belt approaches the surface of Earth down to a few hundreds of kilometers above ground, due to the tilt and shift of the axis of the dipole-like magnetic field of Earth with respect to its axis of rotation. As a consequence, objects in a LEO, in particular the ISS, cross the SAA several times per day and are exposed to the significantly increased particle flux within this region (Fig. 2.6).

Figure 2.7 shows a ten-day average during solar minimum of the differential energy spectra in an ISS like 51.6° inclined orbit at an altitude of 400 km derived from AP8/AE8 (Vette 1991) and AP9/AE9 (Ginet et al. 2013) models in SPENVIS

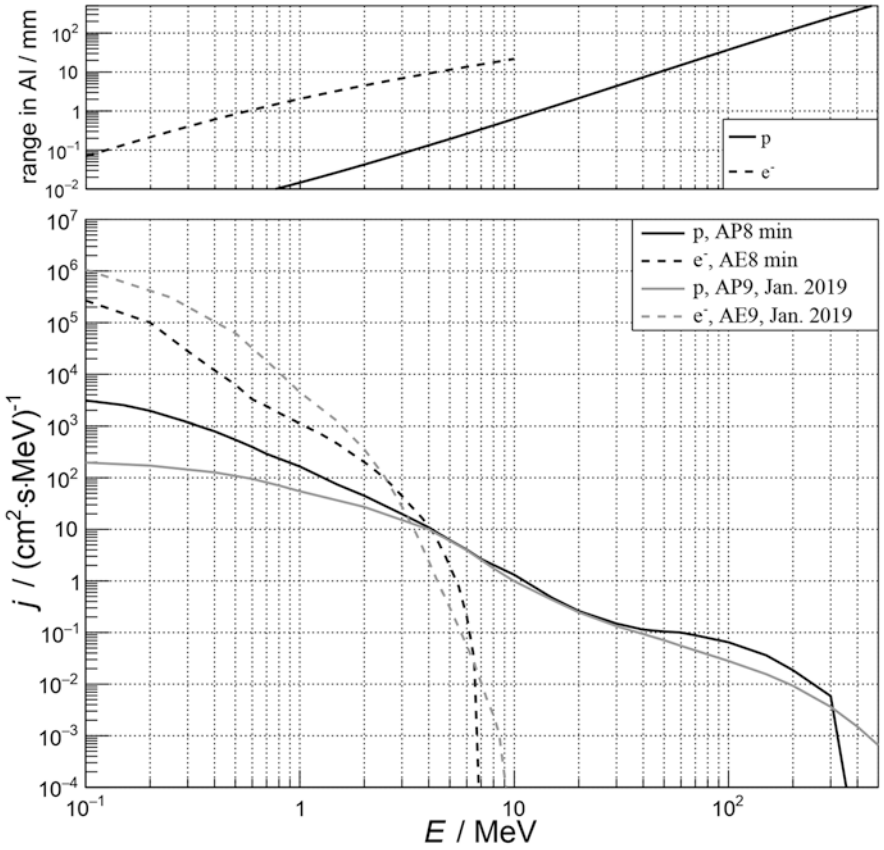

Fig. 2.7 Differential proton (p) and electron (e^-) spectra from AP/AE8 and AP/AE9 models for a 51.6° inclined orbit at an altitude of 400 km (bottom) and the corresponding particle ranges in aluminum (top)

(www.spenvis.oma.be). The respective range of protons and electrons in aluminum is illustrated in the top panel. The trapped particle environment encountered in this orbit, according to the models, contains protons with energies up to several hundred MeV from the inner radiation belt in the SAA (cf. Fig. 2.6) and electrons with energies up to almost 10 MeV mostly from the outer radiation belt.

Electrons below a few MeV are stopped by a few millimeters of aluminum while radiation belt protons at their highest energies can penetrate several centimeters of shielding. In combination with the fact that the electron intensity drops extremely fast by several orders of magnitude between 1 and 10 MeV means that an increase in dose from electrons is not observable at the ISS orbit inside the station while the contribution of the trapped protons to the absorbed dose can reach 50% and more.

2.2 Radiation Dosimetry

2.2.1 Dose Quantities

A framework of dosimetric quantities, definitions, and recommendations concerning radiation protection has been established and continuously developed by the International Commission on Radiological Units and Measurements (ICRU) and the International Commission on Radiological Protection (ICRP). This chapter summarizes the most important quantities relevant for space exploration: relevant reports are: "The 2007 Recommendations of the International Commission on Radiological Protection" (ICRP 2007), "Assessment of Radiation Exposure of Astronauts in Space" (ICRP 2013), "Adult Reference Computational Phantoms" (ICRP 2009), and "Fundamental Quantities and Units for Ionizing Radiation (Revised)" (ICRU 2011). Here, only the most relevant quantities are introduced and the interested reader is referred to the ICRU and ICRP reports for further detail.

On Earth, radiation protection is based on effective dose and ambient dose equivalent, for instance, for the exposure to cosmic radiation in aviation (ICRP 2016). In space, however, effective dose is not applicable due to the use of a single radiation weighting factor $w_r = 20$ for heavy ions which is not generally a valid choice for highly energetic nuclei from GCR (ICRP 2013). Instead, the use of effective dose equivalent is recommended which is based on the quality factor Q rather than radiation weighting factors. No operational dose quantity has been found to be applicable to the exposure to cosmic radiation in space by the ICRP.

The basic quantity in dosimetry on which many of the derived quantities in radiation protection are based on, is the absorbed dose D which is defined through ε, the energy imparted in a volume of mass m. Absorbed dose is defined as:

$$D = \frac{d\varepsilon}{dm} \tag{2.1}$$

The unit of the absorbed dose is J/kg ≡ Gy (gray).

The absorbed dose in macroscopic volumes can be derived by integrating over the volume of interest. If the target volume is a certain type of tissue or organ T in the human body, the absorbed dose in this volume is denoted D_T.

To consider the biological relevance of different types of radiation, the quality factor Q is introduced and the dose equivalent H is defined as:

$$H = Q \bullet D \tag{2.2}$$

The unit of the absorbed dose is J/kg ≡ Sv (sievert).

Equivalently, if the absorbed dose in a tissue T is considered, the corresponding dose equivalent is calculated as $H_T = \bar{Q} D_T$, where $\bar{Q}$ is the mean quality factor in the tissue. The quality factor as defined by (ICRU 1986; ICRP 1991) is a dimensionless factor, solely depending on the linear energy transfer of the particle depositing

the energy. The linear energy transfer L_{Δ} or equivalently, the restricted linear electronic stopping power, is defined in ICRU (2011) as "the quotient of dE_{Δ} by dl, where dE_{Δ} is the mean energy lost by the charged particles due to electronic interactions in traversing a distance dl, minus the mean sum of the kinetic energies in excess of D of all the electrons released by the charged particles":

$$L_{\Delta} = \frac{dE_{\Delta}}{dl} \tag{2.3}$$

The unrestricted linear energy transfer $L_{\infty} \equiv L$ is identical to the electronic stopping power. Based on this definition, the quality factor Q has been defined as a continuous function of L (or LET) in water in ICRP 1991:

$$Q(L) = \begin{cases} 1, \text{if } L < 10\,\text{keV}/\mu m \\ 0.32L - 2.2, \text{if } 10 \le L \le 100\,\text{keV}/\mu m \\ 300/\sqrt{L}, \text{if } L > 100\,\text{keV}/\mu m \end{cases} \tag{2.4}$$

The quality factor is unity for all low L particles, such as electrons and positrons, mostly one for muons, pions, and can become larger for protons and heavier nuclei. The maximum quality factor of 30 is reached at 100 keV/μm.

The quality factor at a point in tissue is defined in ICRP (2013) as

$$Q = \frac{1}{D} \int_{\infty}^{L=0} Q(L) D_L dL \tag{2.5}$$

where D is the absorbed dose in tissue and $DL = dD/dL$ is the distribution of D in L (for charged particles in water) at the point of interest.

Based on the dose equivalent, the ICRP defines the whole body quantity effective dose equivalent H_E which is a weighted sum over the organ dose equivalents using the tissue weighting factors w_T (Eq. 2.7). Other than in terrestrial radiation protection for which the use of the effective dose is recommended, ICRP (2013) recommends to use the effective dose equivalent in the cosmic radiation field in space.

The most recent tissue weighting factors (Table 2.1) introduced in ICRP (2007) are age and sex averaged; the weighting factors are based on experimental data covering stochastic effects (radiation-induced cancer and heritable diseases).

The effective dose equivalent is defined as:

$$H_E = \sum_T w_T H_{T,Q} = \sum_T w_T Q_T D_T \tag{2.6}$$

where the sum is over all tissues T listed in Table 2.1 and Q_T and D_T are the organ averaged quality factor and the absorbed dose in the respective tissue.

For a known radiation field, ICRP (2013) provides fluence-to-dose conversion coefficients for relevant particles, organs, and the total effective dose equivalent for

Table 2.1 Tissue weighting factors w_T recommended by the ICRP

Tissue	w_T	Σw_T
Bone marrow (red), colon, lung, stomach, breast, remainder tissues[a]	0.12	0.72
Gonads	0.08	0.08
Bladder, esophagus, liver, thyroid	0.04	0.16
Bone surface, brain, salivary glands, skin	0.01	0.04
	Total	1.00

From ICRP (2009)

[a]Remainder tissues: Adrenals, Extrathoracic (ET) region, Gall bladder, Heart, Kidneys, Lymphatic nodes, Muscle, Oral mucosa, Pancreas, Prostate (♂), Small intestine, Spleen, Thymus, Uterus/cervix (♀)

a reference anthropomorphic phantom (ICRP 2009) which can be folded with the particle fluence spectra to calculate the dose in the field.

The NASA effective dose as defined in NASA (2013) is not to be confused with the effective dose defined by the ICRP. It is formally identical, however, with the effective dose equivalent concerning the use of quality and tissue weighting factors but with differing numerical values. As stated above, in the ICRP effective dose, the absorbed dose is weighted with radiation weighting factors. NASA applies a risk model that separates the risk of fatal solid cancer and leukemia and the applied quality factors not only depend on the linear energy transfer L but also on the parameter $Z*^2/\beta^2$ with $Z*$ and β being the effective charge number and the particle velocity relative to the speed of light, respectively (Chap. 4). Additionally, the ICRP includes the risk of non-lethal cancer into its gender and age averaged tissue weighting factor while NASAs Q is based on cancer mortality risk.

For the non-stochastic (deterministic) radiation risk, both NCRP (2000) and (ICRP 2013) recommend using the absorbed dose in an organ (D_T) weighted with the relative biological effectiveness (RBE, Sect. 3.3), the gray-equivalent (Gy-Eq). Values for the RBE recommended by ICRP and NCRP to be used in the context of exposure to cosmic radiation are between 1 and 6.

Based on the above introduced quantities, space agencies develop their radiation protection framework and dose limits. For stochastic radiation effects, the Russian, European, and Canadian Space Agencies use the ICRP recommended career limit of 1 Sv. JAXA and NASA, on the other hand, use limits on the Risk of Exposure-Induced Death (REID) which lead to age- and gender-specific limits in the dose. In addition to limits related to stochastic effects, the agencies also introduce dose limits on different organs to consider non-cancer effects; for NASA astronauts, for instance, dose limits for 30 days, one year and the whole career for non-cancer effects are in place (NASA 2014). ESA defines annual limits and for 30 day periods for blood-forming organs, eye and skin (Straube et al. 2010). Current dose limits are summarized in McKenna-Lawlor et al. (2014).

2.2.2 Radiation Detectors and Their Calibration

Dosimetry requires a dedicated radiation detector able to determine the relevant quantities of the radiation field under study. For applications in space radiation dosimetry, the detector system has to be able to measure the relevant radiation protection quantities as defined in the previous chapter, except for the effective dose equivalent which can only be calculated. This implies, that one has to apply detector system being able to measure in what way ever the absorbed dose, the linear energy transfer (LET) spectra and thereby the quality factor of the radiation field as well as the dose equivalent. The effective dose equivalent, on the other hand, would further on be a quantity which can only be measured in space by applying relevant anthropomorphic phantoms.

For the measurement of the space radiation field, one can distinguish between two detector principles. The first detector principle is represented by passive radiation detectors, being able to store the relevant energy deposition from ionizing radiation in their detection material. Examples of passive radiation detectors are thermoluminescence (TL) or optical stimulated luminescence (OSL) detectors as well as Nuclear Track Etch Detectors (CR-39). The second type of instruments are active (in some way powered) instruments which are, for example, based on silicon detectors or on the principle of tissue equivalent proportional counters. Both systems applied have their advantages and disadvantages. While the passive systems have low mass and small dimensions, do not need any external power and data interface and can easily be placed at various positions inside a spacecraft, they do not offer time-resolved data, and they usually have to be returned to the laboratory for evaluation. At the end, they will provide one data value integrated over their respective exposure time.

In contrast to this, the active detector systems enable the investigators to have time-resolved data thereby also having the possibility to resolve the changes of the radiation environment on short time scales—as for example during an SPE. It has to be nevertheless taken into account that the active systems need to be provided with a power and data interface, which can be a demanding task for certain applications. For decades, both of these detector principles have been applied on various space missions and now especially in the frame of the upcoming planned exploration missions to the Moon and in the future to Mars the active detectors will become the main instruments to be applied offering real-time data capabilities as well as possible alarm capabilities for extreme radiation events, as for example an SPE. A relevant summary of instruments applied on-board the ISS as well as for mission to the Moon and Mars is provided in (Berger 2008; Caffrey and Hamby 2011; Narici et al. 2015).

All instruments have in common that they need to be calibrated to the relevant components of the space radiation field. This can be and is accomplished at various facilities around the world offering reference radiation fields for the respective particle species. As for example monoenergetic neutrons are provided at PTB,

Braunschweig, Germany, while the CERF neutron reference field at CERN, Switzerland, provides a neutron spectrum similar to high altitudes.

Of special importance for space are calibrations at facilities offering heavy ions to simulate the GCR environment encountered in space. One of these facilities is the Heavy Ion Medical Accelerator (HIMAC) at the National Institute of Radiological Sciences in Chiba, Japan (Fig. 2.8). Applying the HIMAC facility the space radiation community started in the early 2000 the ICCHIBAN project, aiming for a comparison of the properties of passive and active radiation detectors, thereby also enabling to build up a database of relevant instrument properties (Uchihori et al. 2002; Yasuda et al. 2006). In the last 20 years, a lot of effort has been put in the calibration and comparison of various passive (e.g., Berger and Hajek 2008) and active (Berger et al. 2019) radiations detector systems applied in space and almost all of the

Fig. 2.8 Heavy Ion Medical Accelerator (HIMAC) at NIRS, Chiba, Japan. (© Bartos Przybyla, DLR)

active instruments currently applied for radiation measurements on-board the ISS, the Moon or Mars have been calibrated at the HIMAC facility (Benton et al. 2019).

2.2.3 The History of Space Radiation Dosimetry

In 1912, Victor Franz Hess (1912) started his famous balloon flight, which led to the discovery of the galactic cosmic radiation, and resulting in bestowal of the Nobel Prize to V. Hess in 1936. Though at the time of discovery Hess called the radiation, he discovered "Höhenstrahlung" stating (in the original German written manuscript): *"…Die Ergebnisse der vorliegenden Beobachtungen scheinen am ehesten durch die Annahme erklärt werden zu können, daß eine Strahlung von sehr hoher Durchdringungskraft von oben her in unsere Atmosphäre eindringt…*" (*"… The results of the present observation seem to be most readily explained by assuming that radiation of very high penetrating power enters the atmosphere from above, and can still produce a part of the ionization observed in closed vessels at the lower altitudes"*). Figure 2.9 provides the results of his flights showing the ionization rate in dependence on the altitude above sea level.

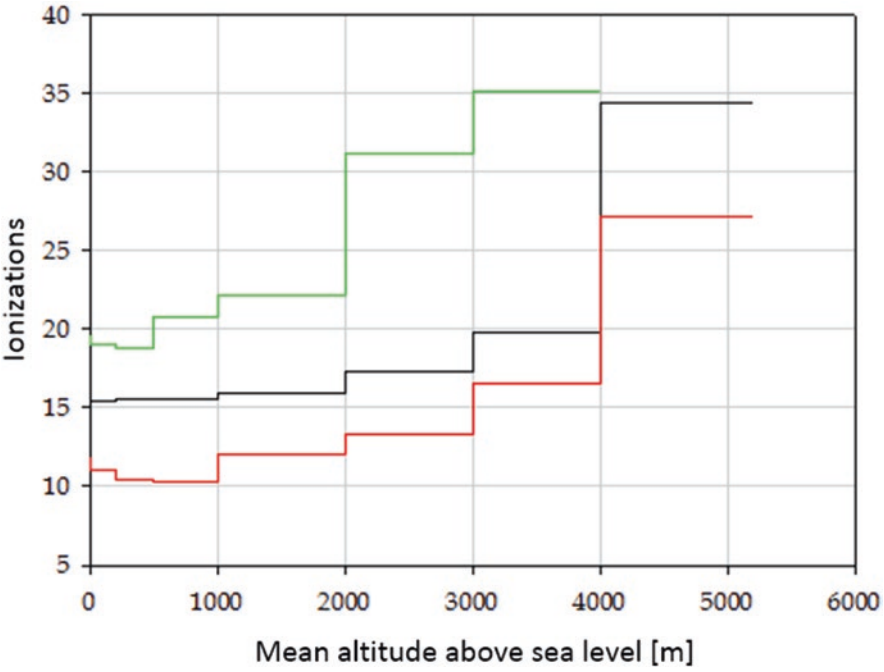

Fig. 2.9 Ionization rate in the atmosphere measured by V. Hess. (Graph drawn based on original data given in Hess 1912)

Further investigations in the coming decades lead to the discovery that these particles are charged ions and that they originate from outside our solar system, which lead in the end to the name cosmic radiation, and to a further Nobel Prize for Cecil Powell in 1950 (Powell 1950). A further historical overview of these endeavors is provided in Carlson (2012). The late 1950s with the International Geophysical Year (IGY) in 1957–1958 led to the discovery of the Earth's radiation belts (Ludwig 1962).

These were discovered by placing various radiation detectors as for example on the US Explorer satellites, which at the end led to the naming of the radiation belts after the main US scientist James Van Allen (Van Allen and Frank 1959; Van Allen et al. 1959a, b). One shall not forget that also Sergei Vernon (Vernov and Chudakov 1960) from the Moscow State University placed a Geiger-Müller counter on the Sputnik 2 mission and also came to the same conclusion as James Van Allen (Baker and Panasyuk 2017). So at the beginning of the human space age in the early 1960s, it was clear that Earth was surrounded by radiation belts and also that cosmic radiation impinges on the Earth atmosphere.

Nevertheless, the reason for starting radiation measurements for human space missions in the USA was a different one. The amount of nuclear explosions in the atmosphere (Hess 1964) and the subsequent creation of artificial radiation belts especially after the "Starfish Prime" nuclear explosion in 1962 shortly before the Mercury mission led to the statement *"…the creation of an artificially trapped electron belt by a high-altitude nuclear explosion on July 9, 1962, made it necessary to place radiation dosimeters aboard the spacecraft used in the eight Mercury-Atlas mission (MA-8)…"* (Warren and Gill 1964). This was the starting point of the radiation measurements for human spaceflight. Figure 2.10 shows how the astronauts on the Mercury mission were equipped with passive thermoluminescence detectors on various parts of the body.

From the NASA Mercury mission onwards (Warren and Gill 1964) followed by the Gemini missions (Richmond 1972), all astronauts were equipped with personal passive radiation detectors and additional instruments as nuclear emulsion and ionization chambers were applied within the spacecraft. During the Apollo missions, various experiments were carried out to determine the radiation loads as given in English et al. (1973), Schaefer et al. (1972), and Schaefer and Sullivan (1976).

An overview table of the radiation doses received during the Apollo lunar landing missions is given in Table 2.2, based on the compendium of space-related dosimetry data provided by Benton (1984).

Noteworthy at this point is also that the first German experiment, the Biostack experiment (Buecker et al. 1973) was already flown as part of the Apollo 16 and 17 missions with its aim to correlate the radiation environment outside LEO and its effect on biological samples. The total mission dose measured with this experiment by thermoluminescence detectors was between 5.0 and 6.2 mGy, which is very close to the data provided by the NASA detectors (as given in Table 2.2 for the Apollo 16 mission).

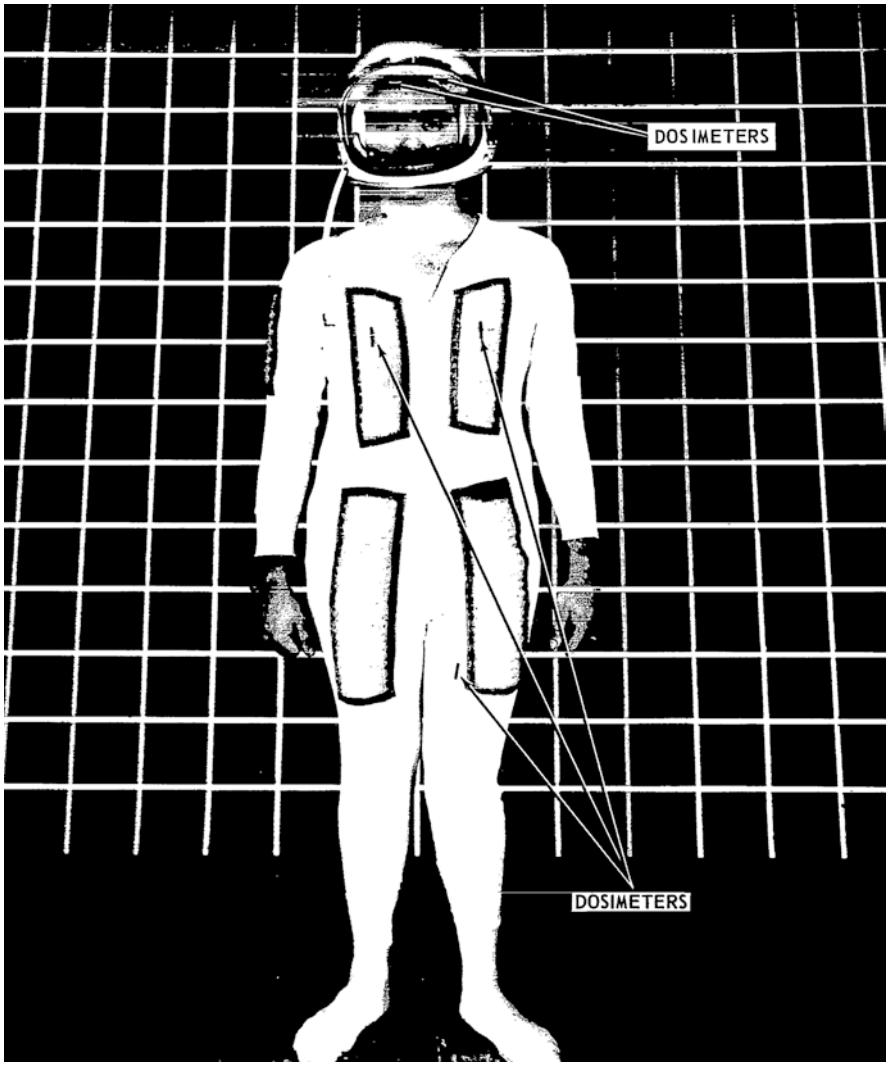

Fig. 2.10 Placement of TLD detectors on the pilot for the Mercury mission. (Warren and Gill 1964)

One should not forget when thinking about the space race to the Moon that also the scientists in Russia were working on radiation detectors and radiation dosimetry for the Russian spacecraft. An overview of data measured during the Vostok, Voshkod (1961 to 1965), and the Soyuz-3 to −9 missions in the years 1968 to 1970 is provided in Benton and Henke (1983). With the start of the NASA Space Shuttle missions, a new spacecraft was available for science, but also as a vehicle for space dosimetry-relevant first data from the STS-1 to the STS-41 missions are

Table 2.2 Overview of Apollo missions

Apollo mission	Duration (hours)	Lunar surface duration	Average radiation dose [mGy]
11	194.0	21 hrs, 38 mins	1.8
12	244.5	31 hrs, 31 mins	5.8
14	216.0	33 hrs, 31 mins	11.4
15	295.0	66 hrs, 54 mins	3.0
16	265.8	71 hrs, 2 mins	5.1
17	301.8	74 hrs, 59 mins	5.5

Data from Benton (1984)

summarized in Benton (1984). The following MIR space station already had radiation instrument (as for example the famous R-16 ionization chamber) installed inside to provide baseline data and possible alarm capabilities for the crew. With the increased cooperation in space, seen for example by the visits of the Space Shuttle to MIR (so-called Shuttle-MIR missions), the amount of groups providing detectors and comparing their results increased. Badhwar et al. (2002) provide a good compendium of all instruments applied within the MIR space station, their properties and provide also an overview and comparison of measured and calculated radiation values for various locations inside the MIR space station. A full comparison of all measurements performed on-board MIR by various institutions is given in the special issue "Radiation on the MIR Space Station" (Radiat Meas. 35, 5, 2002).

With the launch of the ISS at the end of the 1990s radiation detectors were an integrated part of the station in the USA and the Russian segment and were and still are applied as operational detectors together with additional instruments aiming for various scientific radiation research as given in Berger (2008) and Narici et al. (2015).

2.2.4 Human Phantom Experiments

One of the foremost objectives of space radiation dosimetry is to serve as a solid basis for risk assessment for cosmic ray-induced late effects such as cancer, even if the radiobiology associated with these unique radiation fields to a considerable amount is still unknown. The use of dedicated phantoms, simulating a space traveler's body, provides a detailed mapping of dose distribution that is essential for evaluating the doses absorbed in different organs and tissues. Dose measurements are obtained by using a generally large amount of miniature dosimeters, such as thermoluminescence (TL) phosphors, arranged in a regular grid within the mannequin. Due to the considerable mass of such phantom bodies, the number of associated experiments that have actually been conducted in LEO is small. Table 2.3 lists the phantom experiments performed during various space missions.

The experiments started with the first anthropomorphic phantom head on-board a Space Shuttle in the years 1989–1990 (Konradi et al. 1992), followed by the

Table 2.3 Phantom experiments in Space

Experiment	Date	Location
Phantom Head	1989–1990	STS-28 / STS-36 / STS-31
Spherical Phantom	1997–1999	MIR
Anthropomorphic Phantom FRED	1998	STS
Anthropomorphic Phantom FRED	2001	ISS
Spherical Phantom MATROSHKA-R	2004–	ISS
Anthropomorphic Phantom MATROSHKA	2004–2012	ISS

spherical phantom on-board a space station (MIR) in the years 1997–1999 (Berger et al. 2004) and the first exposure of a whole anthropomorphic upper torso in space (Space Shuttle 1998). This space shuttle flight was the first flight, where the effective dose equivalent for a human was determined based on data from radiation detectors placed inside a phantom (Yasuda 2009). This torso (so-called FRED) was also applied for the first torso measurements inside the ISS during Increment 2 in the year 2001. A second—higher developed—spherical phantom (MATROSHKA-R) started its measurement phase inside the ISS in the year 2004 (Kireeva et al. 2007), together with the ESA MATROSHKA (MTR) experiment (outside the ISS in the MTR-I phase) (Reitz et al. 2009). The MATROSHKA experiment was further on also performed inside the Russian part of the ISS in the frame of the MTR-2A and -2B phases and also in the Japanese part of the ISS in the frame of the MTR-2 KIBO experiment. This was the first long-term exposure of a phantom at one hand outside the ISS and on the other hand for three long missions inside the ISS.

As stated before, the ESA MATROSHKA facility and the respective MATROSHKA experiments were the biggest endeavors for the determination of the effective dose equivalent ever accomplished on-board the ISS.

Within the MTR facility thousands of passive thermoluminescence detectors were applied to determine as close as possible the relevant organ doses inside the phantom. In addition, detectors were placed on the surface of the phantom to determine the skin dose (Berger et al. 2013) and the dose equivalent on the surface to have a comparison with the finally determined effective dose equivalent (Puchalska et al. 2014). For more information about the MATROSHKA experiment—see also https://www.fp7-hamlet.eu. Figure 2.11 provides on the left a picture of the MTR facility mounted outside the Russian part of the station in the frame of the MTR-1 experiment and on the right the results for the three-dimensional dose distributions measured during this exposure. These results are the baseline for the calculation of the organ doses and for the further determination of the effective dose equivalent.

In summary it was evaluated that the effective dose equivalent (as given in Table 2.4) for an outside exposure (MTR-1) is a factor of two to three lower than the measured dose on the surface of the body (skin dose) due to the self-shielding of the body for the lower energetic electrons and protons encountered outside the ISS. For an inside exposure, a personal dosimeter would still conservatively overestimate the effective dose equivalent to approximately 20%.

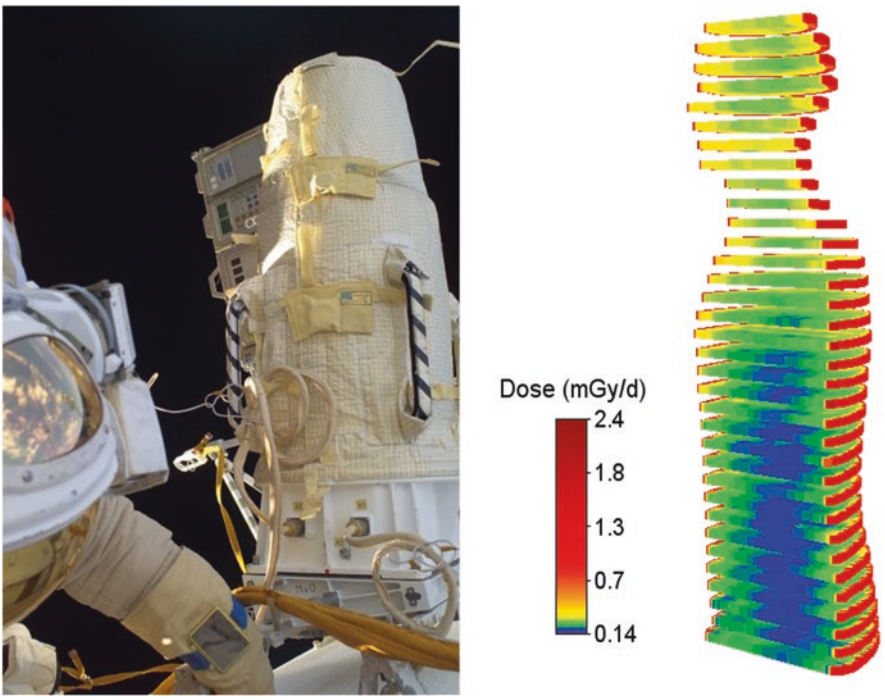

Fig. 2.11 The MTR-1 outside exposure and the 3D dose distribution from the outside exposure. (Data DLR)

Table 2.4 Effective dose equivalent (E) for two MTR experiments

Experiment	E (μSv/d)	Skin dose (μSv/d)
MTR-1 (outside ISS)	722 ± 35	3025 ± 453
MTR-2A (inside ISS)	552 ± 26	641 ± 96

From Puchalska et al. (2014)

2.3 Exposure Scenarios: Measuring and Modeling of Space Radiation

If the radiation exposure in different space scenarios is considered for instance by comparing different measurements or model calculations, it is of paramount importance to keep in mind that the environment is extremely variable in time and space but also strongly depends on the specifics of the dose measurement or calculation. The introduction of a small detector into a radiation field may lead to negligible changes in the field in most cases but the human body, may it be in simulations by means of numerical phantoms, in measurements by means of an anthropomorphic or water phantom or in personal dosimetry, will affect the radiation field and, as a consequence, the dose rates. This effect will be most pronounced in fields which are

dominated by low energy particles, such as most SEP events and outer radiation belt electrons, but is also present for the highly penetrating field of GCR. In an extreme case a small detector may measure extremely high dose values from relatively low energetic particles which would, in case of human exposure, be completely absorbed in the skin and the dose to the more sensitive inner organs may be zero. Additionally, the variation of the radiation field with shielding is not necessarily linear and deriving organ dose values using their average shielding is not always a valid approach.

Many detectors that are applied in dose rate measurements use silicon chips as sensitive volume. The energy deposition of neutrons in silicon, however, is very low compared to water or tissue, the relevant materials for radiation protection. In a situation in which a relevant secondary neutron field exists, the additional contribution from neutrons to the dose in tissue has to be evaluated by other means.

It follows that extreme caution has to be taken if results that have been obtained in one scenario are translated to a different one, for instance, if measurements from a sub-millimeter silicon detector are used to derive organ doses to humans. Additional information about the radiation field, for instance, through model calculations or other types of detectors, is absolutely necessary in such a case.

The following chapter describes different scenarios that are of importance to current human spaceflight or will become important in the near future. In all of these scenarios, astronauts are constantly exposed to GCR and potentially to SEP and, in case of LEO, to charged particles in the radiation belt. Figure 2.12 gives a rough overview over approximate dose rates from GCR that are encountered in different exposure scenarios. It is important to note, however, that in each of these situations, the dose rate can vary significantly, depending for instance on altitude, location, mass shielding, or solar activity.

While there is comprehensive experimental data from the ISS which were recorded under human spaceflight conditions, no such data exist for interplanetary

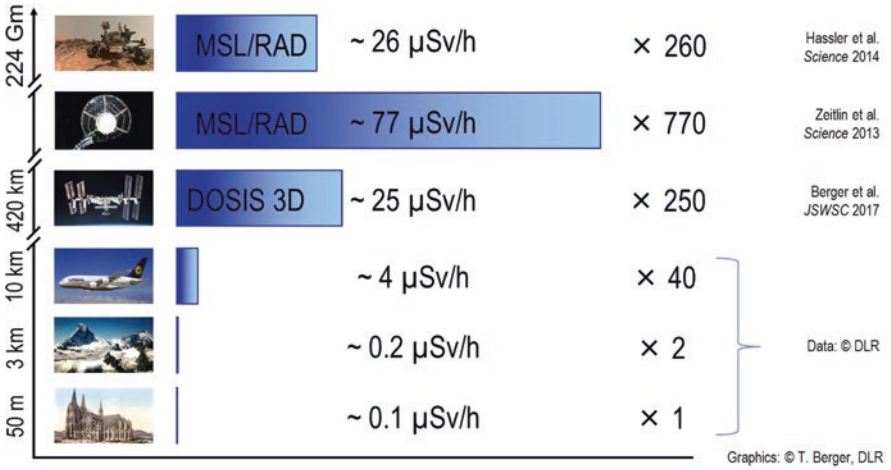

Fig. 2.12 Approximate dose rates in different exposure scenarios

space and the lunar and Martian surface. Available information for these scenarios is restricted to measurements on robotic missions and model estimates.

2.3.1 Low Earth Orbit: The International Space Station

The International Space Station (ISS) is in a LEO at an altitude between approximately 300 km and 400 km and with an inclination of 51.6° which means that it reaches maximum geographic latitudes of 51.6°N and 51.6°S, respectively. Its orbiting period is approximately 90–93 minutes which corresponds to 15.5 to 16 orbits per day. As a consequence, the longitude of the ascending node of the ISS shifts west by approximately 23° for each pass.

The radiation environment to which the ISS and the astronauts are exposed to varies significantly within one orbit but also during one day, when the longitude of the ascending node changes. The underlying mechanism of these variations is the magnetic field of Earth and its effect on charged particles arriving at Earth from interplanetary space and the fact that charged particle populations are trapped within this field. The total exposure of astronauts on the ISS is typically about 200–300 μGy/d and 500–700 μSv/d (Berger et al. 2017); the exact value depends on the local shielding, the point in the solar cycle, the altitude of the station, and other factors.

Astronauts on-board the ISS are protected from GCR and SEPs by two natural mechanisms: The obstruction of the sky by the solid Earth and the shielding provided by the Earth's magnetosphere.

The former can be estimated as follows: If Earth or any other celestial body is approximated by a sphere with radius R, the fraction f of the obstructed sky for an object in an orbit around the body can be expressed as a function of the altitude h of the object above the surface:

$$f = 0.5 \bullet (1 - \cos\left(\arcsin\left(\frac{R}{h+R}\right)\right) \tag{2.7}$$

For a low Earth orbit at $h = 400$ km above ground and a radius between 6357 km and 6378 km (https://nssdc.gsfc.nasa.gov/planetary/factsheet/earthfact.html) this results in $f = 0.331$ (33%) of sky which is blocked, which means that for zero magnetic shielding at high latitudes, the dose rate is expected to be one third lower than in interplanetary space for an identical shielding, if albedo particles from the atmosphere are neglected.

While the magnetic shielding has a negligible effect at high latitudes, it has a significant influence on the radiation field encountered on-board the ISS if the whole orbit is considered. Figure 2.13 shows the effective vertical cut-off rigidity R_C which is a measure of the magnetic shielding effect against charged particles from interplanetary space. The cut-off rigidity can be used as a lower threshold for the rigidity

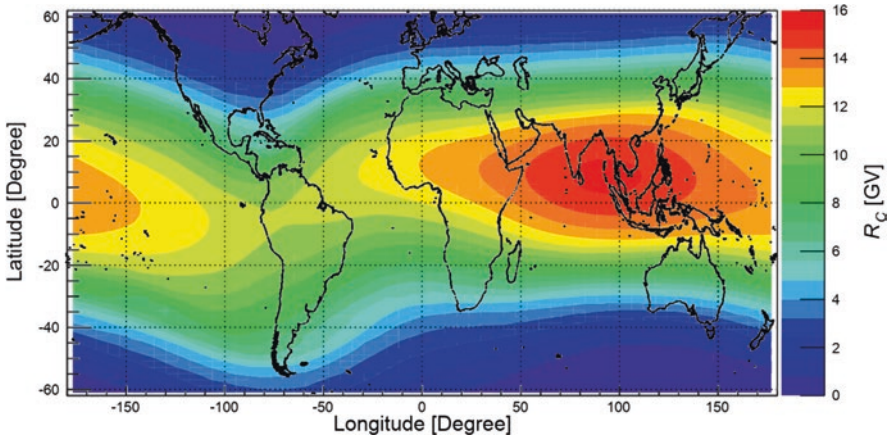

Fig. 2.13 Effective vertical cut-off rigidity R_C at 400 km altitude

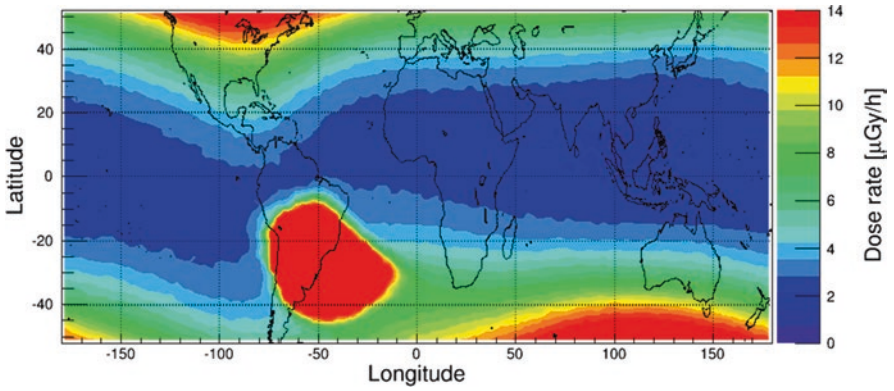

Fig. 2.14 Absorbed dose rates in silicon (Si) measured during solar minimum conditions in 2009 on-board the ISS with the DOSTEL instrument in the DOSIS project. (Berger et al. 2017)

of particles to be able to penetrate the magnetosphere to the given location. The rigidity is defined as the momentum of a particle divided by its charge $R = p/q$.

Additionally, the maximum values at the highest latitudes change during the course of the day and reach their peak values (~15 µGy/h in Si in Columbus during solar minimum) at longitudes around 100°W on the southern hemisphere and around −80°E on the northern hemisphere. As geomagnetic shielding at these positions is negligible for GCR, these values can give an estimate for the dose rates which can be expected in interplanetary space if the geometrical shielding of Earth is considered.

Figure 2.14 (Berger et al. 2017) illustrates the measured dose rates in silicon in the COLUMBUS module of ISS in 2009. The GCR flux in the year 2009 reached an intensity maximum unprecedented in the space age, and it can be considered as a

worst case scenario to our current knowledge. The measured dose rate presented in Fig. 2.14 and its variation, with the exception of the South Atlantic region, are dominated by the GCR and their variation due to the magnetospheric shielding. The shielding at high south-eastern and high north-western latitudes is negligible (cf. Fig. 2.13) and the dose rates from GCR reach their peak values of more than 10 μGy/h which corresponds to about 70% of the value in interplanetary space (due to the obstruction by solid Earth at an altitude of 400 km). At low latitudes along the geomagnetic equator, the magnetic shielding is maximum and the dose rates decrease to below 2 μGy/h. The averaged dose rate from GCR in silicon in 2009 within the COLUMBUS module measured by Berger et al. (2017) was ~160 μGy/d (520 μSv/d, $Q \approx 3.3$). Lishnevskii et al. (2012) determined the dose rate from GCR at different locations in the Russian service module to be between 100 μGy/d and 110 μGy/d in 2009. These values were reached during the solar activity minimum which corresponds to the GCR intensity maximum. During solar maximum, dose rates are significantly lower.

Peak dose rates in the SAA can reach values of several hundred μGy/h but the exact values depend on the trajectory of the station, especially its altitude, the local mass shielding and the solar activity, and they can change during geomagnetic disturbances caused by complex interactions of the interplanetary medium with the magnetosphere. In the relatively heavily shielded environment inside the station, the averaged dose rate from SAA particles in COLUMBUS amounts to approximately 70–100 μGy/d (100–200 μSv/d).

Inside the ISS, the astronauts are effectively shielded from the electrons in the radiation belts which reach maximum energies of a few MeV.

Although measurable in rare events, their contribution to the total dose is negligible. Outside the station, for instance during extra vehicular activities, this changes fundamentally. Dachev (2018) have measured outside the ISS between October 2014 and January 2015 an average dose rate in silicon from outer radiation belt electrons of 278 μGy/d and a maximum value of almost 3 mGy/d. As the electrons have relatively low energies, the dose rate to humans cannot directly be derived from the dose in a thin detector due to the self-shielding of the body.

Sato et al. (2011), however, have estimated by numerical means the contribution of trapped electrons to the dose to astronauts as 0.737 mSv/d for the skin and 0.0232 mSv/d for the effective dose equivalent (note: as the quality factor of electrons is unity, these numbers are identical for the absorbed dose in tissue in mGy/d). Inside the station, the estimates by Sato et al. (2011) are <1 μSv/d for both the effective dose equivalent and the skin dose.

The GCR contributions to the organ doses on-board the ISS during solar minimum for a spherical Al shielding of 20 g/cm^2 have been estimated by Matthiä et al. (2013) to be ~90 μGy/d and 220–260 μSv/d, where the lower values are for the inner organs which benefit more from the self-shielding of the body and for which the quality factor is lower.

Astronauts on-board the ISS are most of the time effectively protected from SEPs by the Earth's magnetic field. Only few events accelerate protons to kinetic

energies above 1 GeV and even those can reach the ISS only at very limited regions at high latitudes at eastern longitudes in the south and at western longitudes in the north. A kinetic energy of 1 GeV corresponds to magnetic rigidity of approximately 1.7 GV for protons which limits the regions accessible to these particles to the purple areas in Fig. 2.13. As a consequence, the effects of SPEs are measurable on the ISS only during short time intervals during an orbit, if at all. Additionally, the onset of an event as measured on-board the ISS can be delayed significantly with respect to the arrival of the energetic particles at Earth due to the fact that it can take hours for the ISS to reach the areas of minimum magnetic shielding. For the most recent ground level enhancement in 2017, the delay between the beginning of the event as measured by satellites in geostationary orbit (GOES) and on the ISS was approximately 12 h (Berger et al. 2018; Matthiä et al. 2018).

Lifting space stations to higher altitudes, for instance, to reduce the atmospheric drag, results in a significantly higher radiation exposure of the astronauts as the area of and the intensity of the particle flux in the crossings of the radiation belt increases. Berger et al. (2017) have measured an increase of the absorbed dose in the SAA in the COLUMBUS module of ISS of almost 100% when the station was lifted to more than 400 km altitude from its earlier 350 km between 2011 and 2013.

Organ doses to astronauts on-board the ISS have been determined experimentally in the MATROSHKA project (Reitz et al. 2009). In the MATROSHKA project, an anthropomorphic phantom equipped with passive and active radiation detectors was exposed outside and at several locations inside the ISS between 2004 and 2011 and measured dose rates between ~0.17 mGy/d and 0.25 mGy/d.

2.3.2 Interplanetary Space

Any spacecraft leaving the Earth's magnetosphere is continuously exposed to the full intensity of GCR and sporadically to SEPs. While astronauts on-board the ISS or any other spacecraft in LEO are effectively protected by Earth itself and its magnetosphere, the only protective mechanism in interplanetary space is the mass shielding provided by the spacecraft itself.

The Radiation Assessment Detector (RAD) (Hassler et al. 2012) of the Mars Science Laboratory (MSL) (Grotzinger et al. 2012) was the first instrument to measure dose rates on a trajectory to Mars between December 2011 and July 2012 during a period of moderate solar modulation. The average dose rate from GCR measured on MSL's cruise was 0.481 ± 0.080 mGy/d in H_2O (0.332 ± 0.023 mGy/d in Si) and 1.84 ± 0.33 mSv/d, corresponding to a quality factor of 3.82 ± 0.25 (Zeitlin et al. 2013). Figure 2.15 illustrates the dose rate in silicon measured by RAD on its interplanetary trajectory to Mars with the underlying relatively constant rates of the GCR and five occurrences of SEP events which manifest in spikes in the dose rate with peak values of up to a few thousand μGy/d.

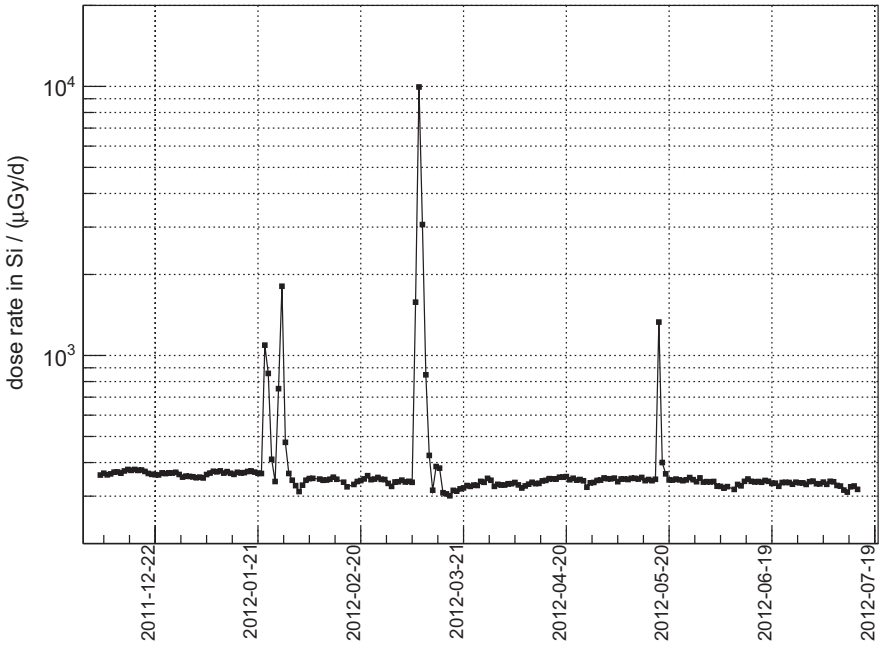

Fig. 2.15 Dose rate measured by the RAD instrument during the transfer of MSL from Earth to Mars (data from Zeitlin et al. 2013)

Semkova et al. (2018) have measured between April and September 2016 at a comparable GCR intensity during the EXO-Mars transit to Mars. The measured GCR dose rates in Si for two different detector configurations were 372 ± 37 μGy/d and 390 ± 39 μGy/d. Other instruments have measured the radiation in lunar transit (Dachev et al. 2011).

These values are approximately factors of 3 to 3.5 greater than what is measured in the COLUMBUS module of ISS during GCR intensity maximum (see Sect. 2.3.1).

These factors contain the influence of the solar modulation, the lack of geomagnetic shielding and shielding by the planet, and differences in the mass shielding provided by the spacecraft and the space station. The most relevant factors are the absence of geomagnetic shielding and the shielding by the planet.

Mass shielding provided by the spacecraft is less effective against GCR and has a major influence mostly on the dose equivalent. The fragmentation of the primary heavy ions leads to a rapidly decreasing quality factor resulting in a drop in dose equivalent for only moderately changing absorbed doses.

A large effort has been undertaken by numerous authors to estimate the radiation exposure from GCR in interplanetary space and the impact and effectiveness of various types of materials (Townsend et al. 1989, 1991; Kim et al. 2010; Mrigakshi et al. 2013b; Slaba et al. 2017; Norbury et al. 2019). Results vary significantly from author to author but are also developing over time. Apart from the shielding geometry and the

GCR boundary condition, the geometry for which the dose was calculated matters. Recently published values by Norbury et al. (2019) for solar minimum under unshielded conditions are 2.5 mSv/d for the dose equivalent in a slab and 1.2 mSv/d for the effective dose equivalent which impressively shows the effect of the self-shielding of the body reducing the exposure by about a factor of two. These results are compatible with results by Kim et al. (2010) and Mrigakshi et al. (2013b). The calculated quality factors are approximately 3 but reducing significantly with increasing shielding.

2.3.3 Moon

Moon lacks both major mechanisms that protect life on Earth from cosmic radiation: an atmosphere and a magnetic field. Astronauts in lunar orbit or on the lunar surface are, except for the shielding provided by any natural or man-made shelter, exposed to the full intensity of GCR and SEPs. In their report on Life Science studies performed during the Apollo missions (NASA 1973), NASA derived average dose values for the different missions between 0.16 rad (1.6 mGy, Apollo 7) and 1.14 rad (11.4 mGy, Apollo 14) and concluded that "radiation was not an operational problem during the Apollo Program." These values include contributions from radiation belt crossings and transfer to a lunar orbit. Most of the dose, however, is contributed by GCR in the lunar orbit or on the surface of the Moon. The report, however, also stated that "it is possible that flares, with the accompanying energetic nuclear particles, might hinder future flights beyond the magnetosphere of the Earth." The lack of an atmosphere means that astronauts which are outside of any habitat, shelter, or vehicle are exposed to the full spectrum of energetic particles and only protected by their space suit.

Due to the absence of atmospheric and magnetic shielding, the exposure to cosmic radiation on the lunar surface is expected to be approximately 50% of the exposure in interplanetary space under comparable shielding conditions if albedo radiation produced in the regolith is neglected. At a given point on the surface, the exposure could be further reduced by nearby rocks, cliffs, crater rims, or other geological formations that reduce the solid angle of open sky. Current measurements are limited to lunar orbit or mission integrated doses from the Apollo missions which also include the transit to the Moon. The first dose rate measurements will be published soon by the Lunar Neutron and Dosimetry (LND) experiment on China's Chang'E 4 lander which started measuring on the lunar surface in January 2019.

Close to the GCR intensity maximum in 2009, the CRaTER instrument on the Lunar Reconnaissance Orbiter Schwadron et al. (2012) measured a dose rate in silicon of 16.5 cGy/year (452 μGy/d) at 10000 km away from the Moon which would result in approximately 8.5 cGy/year (226 μGy/d) on the surface. About one year earlier, the RADOM instrument on Chandrayaan-1 (Dachev et al. 2011) had measured 12.76 μGy/h (306 μGy/d) in silicon (Si) during lunar transfer and 9.46 μGy/h (227 μGy/d) in a 100 km orbit in early 2009. About 34% of the sky are blocked by

the Moon at that altitude which results in an approximate dose rate of 171 μGy/d on the surface. These values are projections of measurements in orbit using simple geometrical considerations. The potential contributions of albedo particles are not considered. Numerical simulations of the albedo radiation estimate a 10% to 25% contribution to the dose or effective dose equivalent (Slaba et al. 2011; Reitz et al. 2012; Spence et al. 2013).

Based on the GCR intensity maximum in late 2009 Reitz et al. (2012) also estimated the organ absorbed dose rates (dose equivalent rates) for an astronaut in a space suit on the lunar surface to reach values between 0.16 mGy (0.44 mSv/d) and 0.22 mGy/d (0.82 mSv/d); the corresponding mean quality factors are between $Q \approx 2.4$ and $Q \approx 4.3$. The corresponding effective dose equivalent was estimated to be 0.6 mSv/d.

2.3.4 Mars

The radiation field at the Martian surface is of great interest as Mars is a potential destination for human missions in the near future, as well. In addition to the transit times in interplanetary space, scenarios for a human mission to Mars typically include a stay on the surface of several months. During this time, the astronauts will be continuously exposed to GCR and its secondary radiation field produced in interactions with the Martian atmosphere and regolith and sporadic SEPs. The atmosphere of Mars consists mostly of CO_2, with some contribution of nitrogen (N), argon (Ar) and trace gases and provides shielding against cosmic radiation corresponding to an areal density of 18–23 g/cm^2, depending on altitude, season, and time of day. This shielding is a mass equivalent of approximately 20 cm of water and significantly lower than the protection that Earth's atmosphere provides, which is about a factor of 50 greater at sea level and still a factor of 10 or more greater at commercial flight altitudes. Nevertheless, the atmospheric shielding on Mars is sufficient to alter the primary GCR field drastically. A large fraction of the heavy ions of the GCR suffers fragmentation before it reaches the surface which leads to a significant decrease in the contribution of heavy ions to the dose and the intensity of high-LET particles and a simultaneous drop in the quality factor. On the other hand, a secondary radiation field develops which contains a substantial amount of secondary neutrons with a high quality factor.

The Radiation Assessment Detector (RAD) on the Mars Science Laboratory mission measured a decrease in the quality factor from $Q = 3.82 \pm 0.30$ in cruise to 3.05 ± 0.26 on the surface. The corresponding measured absorbed dose and dose equivalent rates on the Martian surface were 0.21 ± 0.04 mGy/d and 0.64 ± 0.12 mSv/d.

Recently, there has been a substantial effort to compare and improve numerical models for the prediction of the radiation field and exposure on the Martian surface using RAD data (Matthiä et al. 2016; de Wet and Townsend 2017; Flores-McLaughlin

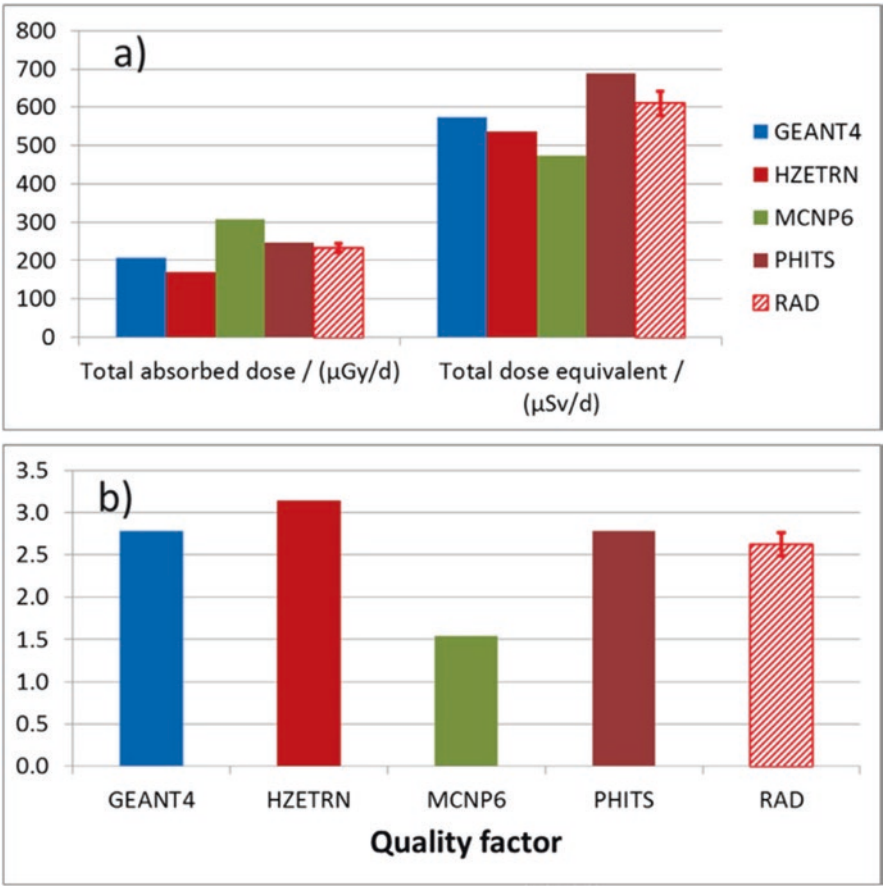

Fig. 2.16 Dose rates (**a**) and corresponding quality factor (**b**) from GCR as measured by the RAD instrument and calculated with different particle transport codes on the surface of Mars for the period between 15 Nov 2015 and 15 Jan 2016. (From Matthiä et al. 2017)

2017; Matthiä and Berger 2017; Ratliff et al. 2017; Slaba and Stoffle 2017). Figure 2.16 summarizes the absorbed dose and dose equivalent rates and the corresponding quality factor of several models in comparison to the RAD measurements. Contributions of different particle types to the absorbed dose and dose equivalent as predicted by GEANT4 model calculations are illustrated in Fig. 2.17. The importance, especiallEq. 2.7y for the dose equivalent, of neutrons produced in the atmosphere and the Martian regolith is evident.

The dose rates in Fig. 2.16 are calculated for a slab of tissue and the values for dose rates in human organs in the identical radiation field are expected to be lower due to the self-shielding effect of the body.

Simonsen et al. (1990) estimated a skin dose equivalent of approximately 0.31 mSv/d to 0.36 mSv/d on the Martian surface. Applying fluence to dose

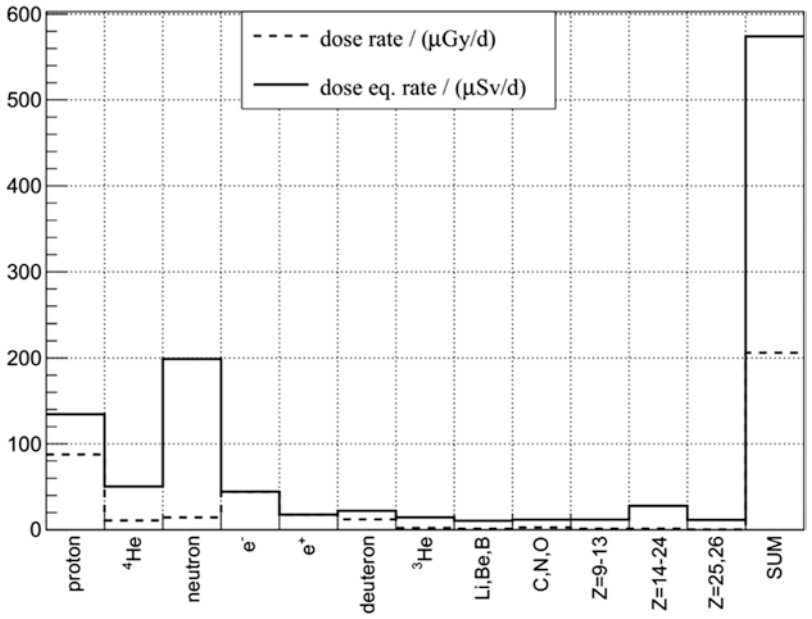

Fig. 2.17 Calculated absorbed dose rates and dose equivalent rates from GCR on the surface of Mars in a slab of tissue from different types of particles (From Matthiä and Berger (2017)) The results have been calculated with GEANT4 for the period between 15 Nov 2015 and 15 Jan 2016

equivalent conversion factors (ICRP 2013) to the results by Matthiä and Berger (2017) gives values of 0.43 mSv/d for the skin and 0.37 mSv/d for the sex-averaged effective dose equivalent.

2.3.5 Solar Particle Events

Solar particle events (SPEs) are highly variable in intensity, energy range, and duration and they are unpredictable. The exposure from each individual event is again strongly dependent on a number of factors, e.g., location of the spacecraft, mass shielding by spacecraft, atmosphere or habitat, magnetic shielding in a planetary magnetosphere, etc. Under such conditions, it is obvious that general conclusions are difficult to draw. Possible ways to address the issue is using a probabilistic approach or defined reference events. Townsend et al. (2018) proposed such a reference event as design basis for missions beyond LEO based on the sum of the October 1989 events. The authors estimated the dose for such an event under unshielded conditions to reach more than one Gy-Eq for both male and female blood-forming organs (BFO, Sect. 3.4) which is a factor of four above the current NASA limit for short-term exposure. They estimated that aluminum shielding of 12 g/cm^2 (for a male) or 15 g/cm^2 (for a female) or polyethylene shielding of 8 g/cm^2 (for a male)

or 10 g/cm^2 (for a female) were necessary to reduce the exposure to not exceed the limit. Kim et al. (2017) concluded in their investigation that 5 g/cm^2 shielding is sufficient to keep the BFO dose below the limit for most events but also, that for rare events a shielding above 15 g/cm^2 is necessary. For EVA conditions, they estimated a total event BFO dose of more than 800 mGy-Eq.

During the recent GLE in Sep 2017, Schwadron et al. (2018) estimated a dose of 0.8–0.9 Gy on the lunar surface, while the same event resulted in a dose of 0.418 mGy in silicon measured by RAD on Mars (Zeitlin et al. 2018). An analysis of the event shows that this significantly lower dose measured on the Martian surface is mostly due to the atmospheric shielding but also caused by different event characteristics, i.e., later onset and different spectral shape (Matthiä et al. 2018). Measurements on the ISS showed even lower values caused by a combined mass and magnetospheric shielding effect (68 μGy and 146 μGy for two differently shielded positions, c.f. (Berger et al. 2018). The event is an excellent example showing how the same event can lead to a wide range of different doses, depending on the local shielding environment but also on the location of the observer relative to the source of the energetic particles.

Generally, in LEO and under atmospheric shielding, even such light shielding as provided by the Martian atmosphere, SPEs are of little relevance for human exposure. Only very few strong events have been observed on MIR and ISS in LEO (Berger et al. 2018). Even the exceptionally strong events in September/October 1989 resulted in a combined measured dose of approximately 35 mGy only. This value is expected to decrease significantly for deeper lying organs; it follows that the BFO dose for the event was at least a factor 10 lower than the short-term exposure limit.

References

Adriani O, Barbarino GC, Bazilevskaya GA, Bellotti R, Boezio M, Bogomolov EA, Bonechi L, Bongi M, Bonvicini V, Borisov S, Bottai S, Bruno A, Cafagna F, Campana D, Carbone R, Carlson P, Casolino M, Castellini G, Consiglio L, De Pascale MP, De Santis C, De Simone N, Di Felice V, Galper AM, Gillard W, Grishantseva L, Jerse G, Karelin AV, Koldashov SV, Krutkov SY, Kvashnin AN, Leonov A, Malakhov V, Malvezzi V, Marcelli L, Mayorov AG, Menn W, Mikhailov VV, Mocchiutti E, Monaco A, Mori N, Nikonov N, Osteria G, Palma F, Papini P, Pearce M, Picozza P, Pizzolotto C, Ricci M, Ricciarini SB, Rossetto L, Sarkar R, Simon M, Sparvoli R, Spillantini P, Stozhkov YI, Vacchi A, Vannuccini E, Vasilyev G, Voronov SA, Yurkin YT, Wu J, Zampa G, Zampa N, Zverev VG (2011) PAMELA measurements of cosmic-ray proton and helium spectra. Science 332(6025):69–72

Aguilar M, Aisa D, Alpat B, Alvino A, Ambrosi G, Andeen K, Arruda L, Attig N, Azzarello P, Bachlechner A (2015a) Precision measurement of the helium flux in primary cosmic rays of rigidities 1.9 GV to 3 TV with the alpha magnetic spectrometer on the international space station. Phys Rev Lett 115(21):211101

Aguilar M, Aisa D, Alpat B, Alvino A, Ambrosi G, Andeen K, Arruda L, Attig N, Azzarello P, Bachlechner A (2015b) Precision measurement of the proton flux in primary cosmic rays from rigidity 1 GV to 1.8 TV with the alpha magnetic spectrometer on the international Space Station. Phys Rev Lett 114(17):171103

Badhwar GD, Atwell W, Reitz G, Beaujean R, Heinrich W (2002) Radiation measurements on the Mir Orbital Station. Radiat Meas 35(5):393–422
Baker DN, Panasyuk MI (2017) Discovering Earth's radiation belts. Phys Today 70(12):46–51
Baker D, Erickson P, Fennell J, Foster J, Jaynes A, Verronen P (2018) Space weather effects in the Earth's radiation belts. Space Sci Rev 214(1):17
Band D, Matteson J, Ford L, Schaefer B, Palmer D, Teegarden B, Cline T, Briggs M, Paciesas W, Pendleton G (1993) BATSE observations of gamma-ray burst spectra. I-spectral diversity. Astrophys J 413:281–292
Benton EV (1984) Summary of current radiation dosimetry results on manned spacecraft. Adv Space Res 4(10):153–160
Benton EV, Henke RP (1983) Radiation exposures during space flight and their measurement. Adv Space Res 3(8):171–185
Berger T (2008) Radiation dosimetry onboard the international Space Station ISS. Z Med Phys 18(4):265–275
Berger T, Hajek M (2008) TL-efficiency—overview and experimental results over the years. Radiat Meas 43(2):146–156
Berger T, Hajek M, Summerer L, Vana N, Akatov Y, Shurshakov V, Arkhangelsky V (2004) Austrian dose measurements onboard Space Station MIR and the international Space Station—overview and comparison. Adv Space Res 34(6):1414–1419
Berger T, Bilski P, Hajek M, Puchalska M, Reitz G (2013) The MATROSHKA experiment: results and comparison from extravehicular activity (MTR-1) and intravehicular activity (MTR-2A/2B) exposure. Radiat Res 180(6):622–637
Berger T, Burmeister S, Matthiä D, Przybyla B, Reitz G, Bilski P, Hajek M, Sihver L, Szabo J, Ambrozova I (2017) DOSIS & DOSIS 3D: radiation measurements with the DOSTEL instruments onboard the Columbus laboratory of the ISS in the years 2009–2016. J Space Weather Space Clim 7:A8
Berger T, Marsalek K, Aeckerlein J, Hauslage J, Matthiä D, Przybyla B, Rohde M, Wirtz M (2019) The German Aerospace Center M-42 radiation detector—a new development for applications in mixed radiation fields. Rev Sci Instrum 90(12):125115
Blasi P (2013) The origin of galactic cosmic rays. Astron Astrophys Rev 21(1):70
Boezio M, Carlson P, Francke T, Weber N, Suffert M, Hof M, Menn W, Simon M, Stephens SA, Bellotti R, Cafagna F, Castellano M, Circella M, De Marzo C, Finetti N, Papini P, Piccardi S, Spillantini P, Ricci M, Casolino M, De Pascale MP, Morselli A, Picozza P, Sparvoli R, Barbiellini G, Bravar U, Schiavon P, Vacchi A, Zampa N, Mitchell JW, Ormes JF, Streitmatter RE, Golden RL, Stochaj SJ (1999) The cosmic-ray proton and helium spectra between 0.4 and 200 GV. Astrophys J 518(1):457–472
Boezio M, Carlson P, Francke T, Weber N, Suffert M, Hof M, Menn W, Simon M, Stephens S, Bellotti R (2000) The cosmic-ray electron and positron spectra measured at 1 AU during solar minimum activity. Astrophys J 532(1):653
Buecker H, Horneck G, Allkofer OC, Bartholoma KP, Beaujean R, Cuer P, Enge W, Facius R, Francois H, Graul EH, Henig G, Heinrich W, Kaiser R, Kuhn H, Massue JP, Planel H, Portal G, Reinholz E, Ruther W, Scheuermann W, Schmitt R, Schopper E, Schott JU, Soleilhavoup JP, Wollenhaupt H (1973) The biostack experiment on Apollo 16. Life Sci Space Res 11:295–305
Caffrey JA, Hamby DM (2011) A review of instruments and methods for dosimetry in space. Adv Space Res 47(4):563–574
Cane HV, Lario D (2006) An introduction to CMEs and energetic particles. Space Sci Rev 123(1):45–56
Carlson P (2012) A century of cosmic rays. Phys Today 65(2):30–36
Dachev T (2018) Relativistic electron precipitation bands in the outside radiation environment of the international space station. J Atmos Solar-Terr Phys 177:247–256
Dachev T, Tomov B, Matviichuk YN, Dimitrov P, Vadawale S, Goswami J, De Angelis G, Girish V (2011) An overview of RADOM results for earth and moon radiation environment on Chandrayaan-1 satellite. Adv Space Res 48(5):779–791

de Wet W, Townsend L (2017) A calculation of the radiation environment on the martian surface, Life Sci Space Res 14:51-56.

Desai M, Giacalone J (2016) Large gradual solar energetic particle events. Living Rev Sol Phys 13(1):3

English RA, Benson RE, Bailey JV, Barnes, CM (1973) Apollo experience report: protection against radiation. NASA TN D-7080

Flores-McLaughlin J (2017) Spherical volume radiation transport simulation of the martian GCR surface flux and dose estimation with PHITS, Life Sci Space Res 14:36-42.

Ginet G, O'Brien T, Huston S, Johnston W, Guild T, Friedel R, Lindstrom C, Roth C, Whelan P, Quinn R (2013) AE9, AP9 and SPM: new models for specifying the trapped energetic particle and space plasma environment. In: The van Allen probes mission. Springer, Boston, MA, pp 579–615

Gopalswamy N, Mäkelä P, Yashiro S, Xie H, Akiyama S, Thakur N (2015) High-energy solar particle events in cycle 24. J Phys Conf Ser 642:012012

Grotzinger JP, Crisp J, Vasavada AR, Anderson RC, Baker CJ, Barry R, Blake DF, Conrad P, Edgett KS, Ferdowski B, Gellert R, Gilbert JB, Golombek M, Gomez-Elvira J, Hassler DM, Jandura L, Litvak M, Mahaffy P, Maki J, Meyer M, Malin MC, Mitrofanov I, Simmonds JJ, Vaniman D, Welch RV, Wiens RC (2012) Mars science laboratory mission and science investigation. Space Sci Rev 170(1–4):5–56

Hassler DM, Zeitlin C, Wimmer-Schweingruber RF, Bottcher S, Martin C, Andrews J, Bohm E, Brinza DE, Bullock MA, Burmeister S, Ehresmann B, Epperly M, Grinspoon D, Kohler J, Kortmann O, Neal K, Peterson J, Posner A, Rafkin S, Seimetz L, Smith KD, Tyler Y, Weigle G, Reitz G, Cucinotta FA (2012) The radiation assessment detector (RAD) investigation. Space Sci Rev 170(1–4):503–558

Hess WF (1912) Über Beobachtungen der durchdringenden Strahlung bei sieben Freiballonfahrten. Phys Z XIII:1084–1091

Hess WN (1964) The effects of high altitude explosions. NASA TN D-2402

ICRP (1991) ICRP Publication 60. The 1990 Recommendations of the International Commission on Radiological Protection. Ann. ICRP 21 (1-3). Smith H (Ed.), Pergamon Press Oxford, New York, Frankfurt, Seoul, Sydney, Tokio

ICRP (2007) ICRP Publication 60. The 2007 Recommendations of the International Commission on Radiological Protection. ICRP Publication 103. Ann. ICRP 37(2-4):1-332. Valentin J (Ed.), Elsevier, Orlando, Amsterdam, Tokyo, Singapore

ICRP (2009) ICRP publication 110: adult reference computational phantoms. Joint ICRP/IRCU report. Ann ICRP 39(2):1–165. Clement CH (Ed.), Elsevier, St. Louis, Oxford, Tokyo, Singapore

ICRP (2013) ICRP publication 123. Assessment of radiation exposure of astronauts in space. Ann ICRP 42(4):1–339. Clement CH, Sasaki M (Eds.), Elsevier

ICRP (2016) ICRP publication 132. Radiological protection from cosmic radiation in aviation. Ann ICRP 45(1):1–48. Clement CH, Hamada N (Eds.), SAGE Publications, London, Thousand Oaks, CA, New Delhi, Singapore, Washington DC and Melbourne

ICRU (1986) Report 40: the quality factor in radiation protection. J ICRU os21(1):1–2

ICRU (2011) Report 85: fundamental quantities and units for ionizing radiation. J ICRU 11(1):1–31

Jentsch V (1981) On the role of external and internal source in generating energy and pitch angle distributions of inner-zone protons. J Geophys Res Space Phys 86(A2):701–710

Jiggens P, Heynderickx D, Sandberg I, Truscott P, Raukunen O, Vainio R (2018) Updated model of the solar energetic proton environment in space. J Space Weather Space Clim 8:A31

Kim M-HY, Hayat MJ, Feiveson AH, Cucinotta FA (2009) Prediction of frequency and exposure level of solar particle events. Health Phys 97(1):68–81

Kim M-HY, Qualls GD, Slaba TC, Cucinotta FA (2010) Comparison of organ dose and dose equivalent for human phantoms of CAM vs. MAX. Adv Space Res 45(7):850–857

Kim M-HY, Blattnig SR, Clowdsley MC, Norman RB (2017) Using spectral shape and predictor fluence to evaluate temporal dependence of exposures from solar particle events. Space Weather 15(2):374–391

Kireeva SA, Benghin VV, Kolomensky AV, Petrov VM (2007) Phantom—dosimeter for estimating effective dose onboard international Space Station. Acta Astronaut 60(4):547–553

Konradi A, Atwell W, Badhwar GD, Cash BL, Hardy KA (1992) Low earth orbit radiation dose distribution in a phantom head. Int J Rad Appl Instrum D 20(1):49–54

Lishnevskii A, Panasyuk M, Benghin V, Petrov V, Volkov A, Nechaev OY (2012) Variations of radiation environment on the international Space Station in 2005–2009. Cosm Res 50(4):319–323

Ludwig GH (1962) The NASA program for particles and fields research in space. NASA TN D-1173

Matthiä D, Berger T (2017) The radiation environment on the surface of Mars—numerical calculations of the galactic component with GEANT4/PLANETOCOSMICS. Life Sci Space Res 14:57–63

Matthiä D, Ehresmann B, Lohf H, Köhler J, Zeitlin C, Appel J, Sato T, Slaba T, Martin C, Berger T, Boehm E, Boettcher S, Brinza DE, Burmeister S, Guo J, Hassler DM, Posner A, Rafkin SCR, Reitz G, Wilson JW, Wimmer-Schweingruber RF (2016) The Martian surface radiation environment—a comparison of models and MSL/RAD measurements. J Space Weather Space Clim 6:A13

Matthiä D, Hassler DM, de Wet W, Ehresmann B, Firan A, Flores-McLaughlin J, Guo J, Heilbronn LH, Lee K, Ratliff H, Rios RR, Slaba TC, Smith M, Stoffle NN, Townsend LW, Berger T, Reitz G, Wimmer-Schweingruber RF, Zeitlin C (2017) The radiation environment on the surface of Mars—summary of model calculations and comparison to RAD data. Life Sci Space Res 14:18–28

Matthiä D, Meier MM, Berger T (2018) The solar particle event on 10–13 September 2017: spectral reconstruction and calculation of the radiation exposure in aviation and space. Space Weather 16(8):977–986. https://doi.org/10.1029/2018SW001921

McKenna-Lawlor S, Bhardwaj A, Ferrari F, Kuznetsov N, Lal AK, Li Y, Nagamatsu A, Nymmik R, Panasyuk M, Petrov V, Reitz G, Pinsky L, Muszaphar Shukor S, Singhvi AK, Straube U, Tomi L, Townsend L (2014) Feasibility study of astronaut standardized career dose limits in LEO and the outlook for BLEO. Acta Astronaut 104(2):565–573

Mrigakshi AI, Matthiä D, Berger T, Reitz G, Wimmer-Schweingruber RF (2013a) How galactic cosmic ray models affect the estimation of radiation exposure in space. Adv Space Res 51(5):825–834

Mrigakshi AI, Matthiä D, Berger T, Reitz G, Wimmer-Schweingruber RF (2013b) Estimation of galactic comic ray exposure inside and outside the Earth's magnetosphere during the recent solar minimum between solar cycles 23 and 24. Adv Space Res 52(5):979–989

Narici L, Berger T, Matthiä D, Reitz G (2015) Radiation measurements performed with active detectors relevant for human space exploration. Front Oncol 5:273

NASA (1973) Biomedical results of APOLLO

NASA (1991) Radiation protection for human missions to the Moon and Mars

NASA (1999) Solar cycle variations and application to the space radiation environment

NASA (2013) Space radiation cancer risk projections and uncertainties—2012

NASA (2014) NASA space flight human-system standard volume 1, Revision A: Crew Health

NASA (2015) Badhwar—O'Neill 2014 galactic cosmic ray flux model description

NCRP (2000) NCRP report 132: radiation protection guidance for activities in low-earth orbit

Norbury JW, Slaba TC, Aghara S, Badavi FF, Blattnig SR, Clowdsley MS, Heilbronn LH, Lee K, Maung KM, Mertens CJ, Miller J, Norman RB, Sandridge CA, Singleterry R, Sobolevsky N, Spangler JL, Townsend LW, Werneth CM, Whitman K, Wilson JW, Xu SX, Zeitlin C (2019) Advances in space radiation physics and transport at NASA. Life Sci Space Res 22:98–124

Powell C (1950) The cosmic radiation. Nobel Lecture

Puchalska M, Bilski P, Berger T, Hajek M, Horwacik T, Korner C, Olko P, Shurshakov V, Reitz G (2014) NUNDO: a numerical model of a human torso phantom and its application to effective dose equivalent calculations for astronauts at the ISS. Radiat Environ Biophys 53(4):719–727

Ratliff HN, Smith MBR, Heilbronn LH (2017) Simulation of the GCR spectrum in the Mars Curiosity rover's RAD detector using MCNP6, Life Sci Space Res 14:43-50.

Reames DV (1999) Particle acceleration at the sun and in the heliosphere. Space Sci Rev 90(3):413–491

Reames DV (2013) The two sources of solar energetic particles. Space Sci Rev 175(1):53–92

Reitz G, Berger T, Bilski P, Facius R, Hajek M, Petrov V, Puchalska M, Zhou D, Bossler J, Akatov Y, Shurshakov V, Olko P, Ptaszkiewicz M, Bergmann R, Fugger M, Vana N, Beaujean R, Burmeister S, Bartlett D, Hager L, Palfalvi J, Szabo J, O'Sullivan D, Kitamura H, Uchihori Y, Yasuda N, Nagamatsu A, Tawara H, Benton E, Gaza R, McKeever S, Sawakuchi G, Yukihara E, Cucinotta F, Semones E, Zapp N, Miller J, Dettmann J (2009) Astronaut's organ doses inferred from measurements in a human phantom outside the international space station. Radiat Res 171(2):225–235

Reitz G, Berger T, Matthiae D (2012) Radiation exposure in the moon environment. Planet Space Sci 74(1):78–83

Richmond RG (1972) Radiation dosimetry for the Gemini program. NASA TN D-6695

Sato T, Endo A, Sihver L, Niita K (2011) Dose estimation for astronauts using dose conversion coefficients calculated with the PHITS code and the ICRP/ICRU adult reference computational phantoms. Radiat Environ Biophys 50(1):115–123

Schaefer HJ, Sullivan JJ (1976) Atlas of nuclear emulsion micrographs from personnel dosimeters of manned space missions. NASA CR-149446

Schaefer HJ, Benton EV, Henke RP, Sullivan JJ (1972) Nuclear track recordings of the astronauts' radiation exposure on the first lunar landing mission Apollo XI. Radiat Res 49(2):245–271

Schwadron NA, Baker T, Blake B, Case AW, Cooper JF, Golightly M, Jordan A, Joyce C, Kasper J, Kozarev K, Mislinski J, Mazur J, Posner A, Rother O, Smith S, Spence HE, Townsend LW, Wilson J, Zeitlin C (2012) Lunar radiation environment and space weathering from the cosmic ray telescope for the effects of radiation (CRaTER). J Geophys Res Planets 117(E12):E00H13

Schwadron NA, Rahmanifard F, Wilson J, Jordan AP, Spence HE, Joyce CJ, Blake JB, Case AW, Wet W, Farrell WM, Kasper JC, Looper MD, Lugaz N, Mays L, Mazur JE, Niehof J, Petro N, Smith CW, Townsend LW, Winslow R, Zeitlin C (2018) Update on the worsening particle radiation environment observed by CRaTER and implications for future human deep-space exploration. Space Weather 16(3):289–303

Semkova J, Koleva R, Benghin V, Dachev T, Matviichuk Y, Tomov B, Krastev K, Maltchev S, Dimitrov P, Mitrofanov I, Malahov A, Golovin D, Mokrousov M, Sanin A, Litvak M, Kozyrev A, Tretyakov V, Nikiforov S, Vostrukhin A, Fedosov F, Grebennikova N, Zelenyi L, Shurshakov V, Drobishev S (2018) Charged particles radiation measurements with Liulin-MO dosimeter of FREND instrument aboard ExoMars trace gas Orbiter during the transit and in high elliptic Mars orbit. Icarus 303:53–66

Simonsen LC, Nealy JE, Townsend LW, Wilson JW (1990) Space radiation-dose estimates on the surface of mars. J Spacecraft and Rockets 27(4):353–354

Simpson JA (1983) Elemental and isotopic composition of the galactic cosmic rays. Ann Rev Nuc Part Sci 33:323–382

Simpson JA (2000) The cosmic ray nucleonic component: the invention and scientific uses of the neutron monitor. In: Cosmic rays and earth. Springer, Dordrecht, pp 11–32

Slaba TC, Blattnig SR (2014) GCR environmental models I: sensitivity analysis for GCR environments. Space Weather 12(4):217–224

Slaba TC, Stoffle NN (2017) Evaluation of HZETRN on the Martian surface: sensitivity tests and model results. Life Sci Space Res 14:29–35

Slaba TC, Blattnig SR, Clowdsley MS (2011) Variation in lunar neutron dose estimates. Radiat Res 176(6):827–841

Slaba TC, Bahadori AA, Reddell BD, Singleterry RC, Clowdsley MS, Blattnig SR (2017) Optimal shielding thickness for galactic cosmic ray environments. Life Sci Space Res 12:1–15

Spence HE, Golightly MJ, Joyce CJ, Looper MD, Schwadron NA, Smith SS, Townsend LW, Wilson J, Zeitlin C (2013) Relative contributions of galactic cosmic rays and lunar proton "albedo" to dose and dose rates near the moon. Space Weather 11(11):643–650

Straube U, Berger T, Reitz G, Facius R, Fuglesang C, Reiter T, Damann V, Tognini M (2010) Operational radiation protection for astronauts and cosmonauts and correlated activities of ESA medical operations. Acta Astronaut 66(7):963–973

Townsend LW, Nealy JE, Wilson JW, Atwell W (1989) Large solar flare radiation shielding requirements for manned interplanetary missions. J Spacecraft Rockets 26(2):126–128

Townsend LW, Shinn JL, Wilson JW (1991) Interplanetary crew exposure estimates for the august 1972 and October 1989 solar particle events. Radiat Res 126(1):108–110

Townsend LW, Adams JH, Blattnig SR, Clowdsley MS, Fry DJ, Jun I, McLeod CD, Minow JI, Moore DF, Norbury JW, Norman RB, Reames DV, Schwadron NA, Semones EJ, Singleterry RC, Slaba TC, Werneth CM, Xapsos MA (2018) Solar particle event storm shelter requirements for missions beyond low earth orbit. Life Sci Space Res 17:32–39

Tylka AJ, Dietrich WF, Atwell W (2010) Assessing the space-radiation hazard in ground-level enhanced (GLE) solar particle events. 2010 Fall AGU Meeting, San Francisco, CA

Uchihori Y, Fujitaka K, Yasuda N, Benton E (2002) Intercomparison of radiation instruments for cosmic-ray with heavy ion beams at NIRS (ICCHIBAN project). J Radiat Res 43(Suppl):S81–S85

UNSCEAR (2000) Sources and effects of ionizing radiation, ANNEX B, Exposures from natural radiation sources. UNSCEAR 2000 REPORT, New York 1: 97–99

Van Allen JA, Frank LA (1959) Radiation around the earth to a radial distance of 107,400 km. Nature 183(4659):430–434

Van Allen JA, McIlwain CE, Ludwig GH (1959a) Radiation observations with satellite 1958 ε. J Geophys Res 64(3):271–286

Van Allen JA, McIlwain CE, Ludwig GH (1959b) Satellite observations of electrons artificially injected into the geomagnetic field. J Geophys Res 64(8):877–891

Vernov SN, Chudakov AE (1960) Investigations of cosmic radiation and of the tab—errestrial corpuscular radiation by means of rockets and satellites. Sov Phys Usp 3(2):230–250

Vette JI (1991) The NASA/national space science data center trapped radiation belt model (1964–1991). National Space Science Data Center (NSSDC), Greenbelt, MD

Warren CS, Gill WL (1964) Radiation dosimetry aboard the spacecraft of the eight Mercury-Atlas mission (MA-8). NASA TN D-1862

Wilson JW (1978) Environmental geophysics and SPS shielding

Xapsos MA, Summers GP, Barth JL, Stassinopoulos EG, Burke EA (2000) Probability model for cumulative solar proton event fluences. IEEE Trans Nuc Sci 47(3):486–490

Yasuda H (2009) Effective dose measured with a life size human phantom in a low earth orbit mission. J Radiat Res 50(2):89–96

Yasuda N, Uchihori Y, Benton ER, Kitamura H, Fujitaka K (2006) The intercomparison of cosmic rays with heavy ion beams at NIRS (ICCHIBAN) project. Radiat Prot Dosim 120(1–4):414–420

Zeitlin C, Hassler DM, Cucinotta FA, Ehresmann B, Wimmer-Schweingruber RF, Brinza DE, Kang S, Weigle G, Böttcher S, Böhm E, Burmeister S, Guo J, Köhler J, Martin C, Posner A, Rafkin S, Reitz G (2013) Measurements of energetic particle radiation in transit to Mars on the Mars science laboratory. Science 340:1080–1084

Zeitlin C, Hassler DM, Guo J, Ehresmann B, Wimmer-Schweingruber RF, Rafkin S, Freiherr von Forstner JL, Lohf H, Berger T, Matthiä D, Reitz G (2018) Analysis of the radiation hazard observed by RAD on the surface of mars during the September 2017 solar particle event. Geophys Res Lett 45:5845–5851